SYNTHESIS AND CHARACTERIZATION OF ALUMINA-DOPED LOW DENSITY POLYETHYLENE (LDPE/ALUMINA) NANOCOMPOSITES

By

Aliyu ABDULRAHEEM

DEPARTMENT OF PHYSICS

AHMADU BELLO UNIVERSITY, ZARIA

NIGERIA.

SEPTEMBER, 2016

SYNTHESIS AND CHARACTERIZATION OF ALUMINA-DOPED LOW DENSITY POLYETHYLENE(LDPE/ALUMINA) NANOCOMPOSITES

BY

Aliyu ABDULRAHEEM

PhD/SCIE/1520/2009-10

A DISSERTATION SUBMITTED TO THE SCHOOL OF POSTGRADUATE STUDIES,

AHMADU BELLO UNIVERSITY, ZARIA

IN PARTIAL FULFILLMENT OF THE REQUIREMENTS FOR THE AWARD

OF

DEGREE OF DOCTOR OF PHILOSOPHY (PhD PHYSICS)

DEPARTMENT OF PHYSICS,

FACULTY OF SCIENCE

AHMADU BELLO UNIVERSITY, ZARIA

NIGERIA

SEPTEMBER, 2016.

DECLARATION

I declare that the work in this research dissertation entitled “Synthesis And Characterization of Alumina-doped Low Density Polyethylene (LDPE/Alumina) Nanocomposites” has been carried out by me in the Department of Physics. The information derived from the literature has been duly acknowledged in the text and a list of references provided. No part of this research dissertation was previously presented for another degree or diploma at this or any other institution.

ABDULRAHEEM Aliyu		
Name of Student	Signature	Date

CERTIFICATION

This project thesis entitled “SYNTHESIS AND CHARACTERIZATION OF ALUMINA-DOPED LOW DENSITY POLYETHYLENE(LDPE/ALUMINA) NANOCOMPOSITES” by ABDULRAHEEM ALIYU meets the regulations governing the award of the degree of PhD Physics of the Ahmadu Bello University, and is approved for its contribution to knowledge and literary presentation

_____ Date: _____

Dr A. A. Abdelghaffar

Chairman, Supervisory Committee

_____ Date: _____

Dr U. Ahmadu

Member, Supervisory Committee

_____ Date: _____

Dr U. Sadiq.

Member, Supervisory Committee

_____ Date: _____

Dr Y. I Zakari

Head of Department

_____ Date: _____

Professor Kabir Bala.

Dean, School of Postgraduate Studies

ACKNOWLEDGEMENT

All praise is due to ALLAH the lord of the worlds Who has made this work a reality. May His everlasting peace and blessings be on His noble apostle whose light will continue to be the source of all illuminations till eternity.

I am sincerely and extremely grateful to my supervisors; Dr A. A. Abdelmalik, Dr U. Ahmadu and Dr U. Sadiq for finding time to render all academic guidance and assistance needed for the completion of this work. They are all worthy academic giants and unique with respect to what they could offer. I pray Allah see them through their individual demands, Ameen.

I am very thankful to all the staff of Physics Department for their individual and collective support throughout my study. The entire staffs of Advanced Physics Laboratory, SHESTCO Abuja are wonderful people especially Mr Noble and Engr Kennneth for all their technical support.

Prof. Abdullahi El-Okene, Prof. Yunusa Bello Prof. Mustapha Gwadabe and Prof. S. O. Idris deserve mention and appreciation for their spiritual and moral support. I am indeed very grateful to my parents, my wives, my children and all my friends for their financial and moral support. May Allah continue to increase them in His blessings and show of mercy wherever they are. Ameen.

Finally, I am very thankful to TETFund and Mac Author Foundation for their financial assistance. I am also thankful to The World Academy of Science (TWAS) for supporting this research.

DEDICATION

This work is dedicated to my spiritual Grandfather Maulana Sheikh Ibrahim Nyass and all the true Lovers of the Holy Prophet (S A W).

ABSTRACT

Nano-sized kaolin also known as alumina was synthesised by acid leaching and subsequently suspended in low density polyethylene (LDPE) to produce nano-polymer for application in electrical insulation. The alumina was prepared by acid leaching via digestion, precipitation, peptization and drying. This was subsequently used to dope the LDPE at varying compositions.

The structural properties of LDPE/γ-alumina with LDPE as a host matrix were investigated by X-ray diffraction, Scanning electron microscopy (SEM) and Fourier Transform Infrared (FTIR) Spectroscopy. Intermediate LDPE/γ-alumina nanocomposites were confirmed by XRD. The Sherrer equation revealed a nano crystalline size of $24.91nm$ for the γ-alumina at 400°C. SEM images also revealed a heterogeneous dispersion of nano particle layers in the LDPE matrix. Uneven dispersion of nano particles was evident due to agglomeration of alumina. The mechanical properties results which were investigated by Nanoindentation showed that the presence of alumina in the LDPE improved the Young's modulus and hardness of the samples. The dielectric permittivity, ac conductivity, relaxation and electrical modulus of the composites were studied in the frequency range of $20\ kHz$ to $180\ kHz$, at room temperature. Addition of alumina up to about 2.5wt% resulted in an increase permittivity.

Doping of LDPE with alumina produced intermediate nanocomposites which possess excellent dielectric properties. The permittivity of LDPE has been measured to be $(2.25 - 2.35)$ at 1 MHz and after doping in this work it was gotten as $(2.85\text{-}3.47)$ at 100 kHz. The mechanical behaviour is practically enhanced by an increase in its hardness from $13.5\ MPa$ to a range of $(14 - 34\ MPa)$ in this work while the elastic modulus is within $(0.74 - 1.44\ GPa)$.

The prepared samples have an average dissipation factor of 0.006228 at 20 kHz. The increase in dielectric permittivity of the samples and relatively low and stable tan delta value is an indication of low loss which makes the material an efficient insulator. The pattern of variation of conductivity of LDPE/alumina with frequency is linear increment and is indicative of the semicrystalline structure of the host matrix. The relaxation behaviour showed the same pattern and have their slopes falling between -0.3593 to -0.5223. This may likely be an indication of low stress and brittle failure which is usually initiated at surface or bulk inhomogeneities that act as stress concentrator and of course which the samples (LDPE/alumina) possess.

Samples doped at 2.5, 3.0 and 3.5 wt% appeared to have most optimum behaviour in that they have the lowest dielectric loss out of all the samples produced. The samples prepared within the stated ranges also have good stability with respect to elastic modulus and hardness and may therefore be considered as a good alternative electronic substrate for polymeric applications compared to others fabricated at different percentage weights.

TABLE OF CONTENTS

LIST OF TABLES

LIST OF FIGURES

LIST OF PLATES

ABBREVIATIONS

NARICT	-	National Research Institute of Chemical Technology
FTIR	-	Fourier Transform Infra-Red
LDPE	-	Low Density Polyethylene
MDPE	-	Medium Density Polyethylene
HDPE	-	High Density Polyethylene
SEM	-	Scanning Electron Microscopy
XRD	-	X-Ray Microscopy
NSM	-	Nano Structured Materials
PNC	-	Polymer Nanocomposites
GN	-	Nanographites
PVA	-	Poly Vinyl Alcohol
HV	-	High Voltage
AC	-	Alternating Current
DC	-	Direct Current
EDL	-	Electric Double Layer
SI	-	System Interntionale
ASTM	-	American Society for Testing and Materials
VNA	-	Vector Network Analyzer
MUT	-	Material Under Test
MH	-	Microidentation Hardness
S/m	-	Siemen per Meter
ev	-	electron Volt
Pa.s	-	Pascal Seconds
Psi	-	pounds per square inches

CHAPTER ONE

INTRODUCTION

1.1 General Introduction

A composite is any material made of more than one component. Composite materials are multiphase materials formed through the combination of materials with different structural, physical and chemical properties. This makes composites different from the other multi-component systems such as blends and alloys. Composites are widely used in such diverse fields as transportation, construction and consumer products (Giannelis, 1996).

Composites offer unusual combinations of component materials properties such as weight, strength, stiffness, permeability, electrical, biodegradability and optical properties that is difficult to attain separately by individual components. A composite material can be fabricated to have specific properties that will meet special requirements. The optimum design of composite component materials and manufacturing process to meet the target properties for specific engineering application is very important (Ali, 2011).

Based on the nature of matrix phase, composite materials can be divided into polymeric, ceramic and metallic composites. Usually the filler phase is embedded to the host matrix phase to make a composite which has properties far from either phase alone. Polymers often have advantages over other materials such as metals and ceramics. They are widely used in various technical applications because of their unique advantages such as ease of production, light weight and ductility. However they have lower mechanical, modulus and strength properties compared to that of metals and ceramics. The commercial importance of polymers and their increasing use, results to the continuous demand for improvement in their properties to meet the necessary

conditions. By the composite technology, polymer properties are improved while maintaining their light weight and ductile nature (Jordan *et al*., 2005).

Nanotechnology is the technology that deals with the synthesis of nano-particles, processing of the nano materials and their applications. Normally, if the particle sizes are in the 1-100nm ranges, they are generally referred to as nano-particles. On the other hand, nanocomposites by definition contain nano-particles of less than 1000 nm in a host matrix. (Fahrner, 2005).

Generally the term nanocomposites materials has broadened significantly over the years to encompass a large variety of systems such as one-dimensional, two-dimensional, three-dimensional and amorphous materials, made of distinctly dissimilar components and mixed at the nanometre scale.

The general class of polymer nanocomposites is a fast growing area of research. Significant effort has been focused on the ability to obtain efficient reproducible nanoscale structures through innovative synthetic approaches. This is because the properties of nano-composite materials depend not only on the properties of the parent constituent material or matrix but also on their morphology and interfacial characteristics (Rao *et al,* 2004). Also from Carl (2002), the properties of nanostructured materials (NSMs), depend on the following four common microstructural features: (i) fine grain size and size distribution; (ii) the chemical composition of the constituent phases; (iii) the presence of interfaces, more specifically, grain boundaries, heterophase interfaces, or the free surface; and (iv) interactions between the constituent domains. The presence and interplay of these four features largely determine the unique properties exhibited by any NSM.

In recent times, there has being a lot of scientific and industrial interests in polymer nanocomposites. This is because they often exhibited remarkable improvement in materials properties when compared to virgin polymer or conventional composites.

Kaolin on the other hand, which is sometimes referred to as kaolinite is a clay mineral, part of the group of industrial minerals, with the chemical composition $Al_2Si_2O_5(OH)_4$. As a layered silicate mineral, it possesses one tetrahedral sheet linked through oxygen atoms to one octahedral sheet of alumina octahedral. Upon calcinations at about 1050℃ via metakaolin between 870-950℃, it transforms to mullite which could be used as an Insulator and related electronic substrate (Encyclopedia Britannica, 2003).

However in recent years the characterization and control of structures at the nanoscale have been studied, investigated and exploited from the natural surroundings. Consequently the nanocomposite technology has emerged as an efficient and powerful strategy to upgrade the structural and functional properties of synthetic polymers. This is the new nanocomposites science, so referred recently in nanotechnology, and was started by the Toyota report (Usuki *et al*., 1993) on the superior improvement in the properties of nylon-6 by the preparation of exfoliated nylon-6/clay nanocomposites and has been continued by more recent studies with carbon nanotubes, carbon nanofillers, exfoliated graphite, nanocrystaline metals and fibers modified with inorganic fillers used in polymeric composites (Paul *et al*, 2008).

Polymer nanocomposites have attracted great attention across the globe academically and industrially due to the exhibition of superior properties such as modulus, strength, toughness and barrier far from those of conventional micro composites and comparable with those of metals. However polymer nanocomposites have added advantage of lower density and ease of processability. In polymer nanocomposites, the filler has at least one dimension in the nanometer

scale and its nanoscale dispersion within the polymer matrix leads to the tremendous interfacial contacts between the polymer and inorganic filler which makes it have more superior properties than those of bulk polymer phase. When the dimensions of filler particles are decreased to the nanoscale, their properties change also significantly (Kumar *et al*., 2009).

Clays are one group of nano-fillers which have been widely used for the preparation of polymer nanocomposites. Recently there has been a growing interest in the development of polymer/clay nanocomposites due to their dramatic improved properties compared to the conventionally filled polymers in a very low fraction of filler addition (LeBaron *et al*., 1999; Thostenson *et al*., 2005). Polymer/clay nanocomposites have received intense attention and research interest driven by the unique properties which can never be obtained by micro size fillers or especially by other nanofillers. The value added properties enhanced without sacrificing the pure polymer processability, mechanical properties and light weight, make the clays more and more important in modern polymer industry.

The preparation of polymer/clay nanocomposites with good dispersion of clay layers within the polymer matrix is not possible by physical mixing of polymer and clay particles. It is not easy to disperse nanolayers in most polymers due to the high face to face stacking of layers in agglomerated tactoids and their intrinsic hydrophilic nature which make them incompatible with hydrophobic polymers. Only a few hydrophilic polymers such as poly (ethylene oxide) and poly (vinyl alcohol) can be miscible with clay nanolayers (Pavildou and Papaspyrides, 2008).

The intrinsic incompatibility of hydrophilic clay layers with hydrophobic polymer chains prevents the dispersion of clay nanolayers within polymer matrix and causes to the weak interfacial interactions. Incompatibility and weak interfacial interactions hinders the exfoliation and preparation of dispersed stable nanocomposite with improved properties. Modification of

clay layers with hydrophobic agents is necessary in order to render the clay layers more compatible with polymer chains. This is a surface modification which causes the reduction of surface energy of clay layers and matches their surface polarity with polymer polarity. The organoclays with lowered surface energy are more compatible with polymers and polymer molecules are able to intercalate within their interlayer space or galleries under well defined experimental conditions.

The surface modification of clay layers can be achieved through a cation exchange process by the replacement of sodium and calcium cations present in the interlayer space or clay galleries by alkylammonium or alkylphosphonium (onium) cations (Ahmad *et al*., 2009). In addition to the surface modification and increasing the hydrophobic nature of clay layers, the insertion of alkylammonium or alkylphosphonium cations into the galleries causes some degree of increase in the interlayer spacing which promotes the intercalation of polymer chains into the galleries during nanocomposites preparation (Chigwada *et al*., 2006).

However, many clay materials have been used on many polymers and many are still been used. The common clays used are the smectite clays comprising of montmorillonite, Hectite and Saponite outlined in the table below

Table 1.1 Chemical structure of commonly used smectite type clays, (Pavlidou & Papaspyrides, 2008).

Smectites	Chemical Formula
Montmorillonite	$M_x(Al_{4-x}Mg_x)Si_8O_{20}(OH)_4$
Hectite	$M_x(Mg_{6-x}Li_x)Si_8O_{20}(OH)_4$
Saponite	$M_xMg_6(Si_8\text{-}xAl_x)O_{20}(OH)_4$

M: monovalent cation, x: degree of cations isomorphous substitution in octahedral sheets. Of the smectite, montmorillonite has been used more among the others due to ease in processing, availability, well known intercalation/exfoliation chemistry, high surface area and high surface reactivity. Kaolin has been thought to have a greater advantage over Montmorillonite because it's more available in Nigeria and when calcined, it will have more high surface reactivity than montmorillonite (Raw Material Research and Development Council, 1997).

Since the remarkable properties of conventional composites are mainly due to interface interactions, the materials dealt with here (Low Density Polyethylene/Alumina) could provide good model systems in which such interactions can be studied in detail using conventional bulk sample (as opposed to surface) techniques. By judiciously engineering the polymer-host interactions, nanocomposites may be produced with a broad range of properties. Daniel *et al* (1999), showed that a comparable mechanism for improving the mechanical properties of ceramics may exist for ceramic matrices, utilizing coherent, nanometer-sized inclusions within the ceramic matrix. This expectation they said is supported by studies on ceramic nanocomposites, for which significant increases in strength are observed in samples containing nano-sized inclusions within the grains or at the grain boundaries of the matrix phase. Inorganic

layered materials exist in great variety. They possess well defined, ordered intralamellar space potentially accessible by foreign species. This ability enables them to act as matrices or hosts for polymers, yielding interesting hybrid nano-composite materials (Hari 2002).

Nano-composites can be divided into two distinct classes, intercalated and exfoliated. In the former, the polymer chains alternate with the inorganic layers in a fixed compositional ratio and have a well defined number of polymer layers in the intralamellar space. In exfoliated nano-composites the number of polymer chains between the layers is almost continuously variable and the layers stand >100 Å apart. The intercalated nano-composites are also more compound-like because of the fixed polymer/layer ratio, and they are interesting for their electronic and charge transport properties. On the other hand, exfoliated nano-composites are more interesting for their superior mechanical properties (Valavala and Odegard, 2005).

1.2 Research Problem

Nanocomposites materials hold the potential to redefine the field of traditional composite materials both in terms of performance and potential applications. There are speculations whether or not polymer nanocomposites have tremendous market potential both as replacements for current composites and in the creation of new markets through their outstanding properties. This is because developing the processing via manufacturing technologies in terms of quantity and value for commercialization will be one of the biggest challenges.

The major problems polymer nanocomposites (PNC) wish to address are cost, weight and efficiency. In recent times, LDPE/clay nanocomposites have emerged to solve these issues owing to their abundance availability. All efforts made in the past by several doping mechanisms are tailored towards addressing these key issues. There has been enhancement of the dielectric

strength from the works of Chanmal and Jog, (2009), while PVDF still retained its flexibility. Since higher enhancement is still required, more research works are needed to be carried out to come up with LDPE/clay with a better enhancement. All clay types have to be completely explored to ascertain which gives the most optimum enhancement.

Low Density Polyethylene/Alumina nanocomposites are thought to possess the property of retaining its flexibility from the ideas raised from the works of Chanmal and Jog, (2009), in the case of PVDF/cloisite while achieving high dielectric constant. LDPE/alumina may be potential candidates for achieving this high dielectric strength and other related advantages. On this premise, Fothergill *et al*, (2003) has postulated that even a 10% improvement in an electrical property such as dielectric strength would have enormous commercial impact worldwide from their commercial point of view. Because of the light nature of alumina in terms of weight, availability and cheapness, LDPE/alumina nanocomposite may be the cheapest compared to the available PVDF/Montmorillonite and that of PVDF/Cloisite nanocomposites.

1.3 Justification

For decades, the electric and dielectric properties of materials have been of immense interest to scientists and researchers. As technology evolved, materials have become progressively more complex, and to optimize performance, their composition, method of production, and diverse performance characteristics must be considered. The key factors of consideration in a material among others are light weight and cost reduction. The LDPE/alumina stands a better chance to address these key issues in polymer nanocomposites (PNC).

From the chemical composition of kaolin that gave rise to the production of alumina, it appears to be lighter in weight than the Montmorillointes that are commonly used. Because of this, kaolin

may go as far as 6%wt doping as against Montmorillonite that could only go as far as 5%wt doping (Umasankar *et al*, 2007 & Song *et al*, 2007). According to the Raw Material Research and Development Council (1997), kaolin of good quality in millions of tonnage can be sourced from various locations in the country. Kaolin which is the starting material of alumina therefore appears to be more available than montmorillonite in Nigeria implying that the cost of Kaolin will be cheaper than that of montmorillonite. Beneficiating kaolin can be manually done and easy, implying that it is very cheap and has a great potential application because of its availability.

1.4 Aim and Objectives

The aim of this work is to synthesis and characterizes low density polyethelene/ alumina nanocomposites suitable for insulation in coaxial cables for radar apparatus, television and premium wires.

The objectives of this work are to:

- Evaluate the morphology and the extent of dispersion of the nano-particles to ascertain the microstructure of the alumina.
- Determine the mechanism by which the nano-particles interact with the polymer matrix.
- Determine the influence of the introduced nano-particles on the mechanical properties.
- Evaluate the dielectric behaviour of the composite material at room temperature.
- Examine the functional groups and bonds appearing in the samples after doping in order to ascertain how much the alumina has influenced the LDPE matrix

1.5 Previous Works

Priya and Jog, (2002 & 2003), were the first to prepare Polymer–clay nanocomposites. They observed from the modified Cloisite used that the addition of organically modified clay resulted in the formation of the β-phase instead of the α-phase upon melt processing. From the work of Umasankar *et al* (2007), their result revealed that the PVDF/Montmorillonite prepared by melt mixing formed β-phase crystals in the presence of organically modified clay when crystallized from its melt and in contrast, α-crystals were formed in the absence of clay and with unmodified clay. As expected, the dielectric constant values for organoclay nanocomposites are found to be higher than the PVDF and PVDF with unmodified clay.

Jeffrey *et al*, (2005), provides an overview of the processing techniques and trends in the mechanical behaviour and morphology of nanocomposites. In general, the material properties of polymer nanocomposites are superior to the pure polymer matrix or composites with larger sized inclusions. The effects of the nanoparticles are dependent on many variables but especially upon the relative crystalline or amorphous nature of the polymer matrix as well as the interaction between the filler and matrix. (Liqiang and seong, 2008), also in their work, Preparation and characterization of polyethylene (PE)/clay nanocomposites by *in situ* polymerization with vanadium-based intercalation catalyst, successfully carried out complete exfoliation of clay during Vanadium-based Zigler-Natta polymerization of ethylene. Even though the mechanical properties of the PE/clay nanocomposites have a noticeable improvement when the clay was exfoliated and well dispersed in the PE matrix, improvement in the electrical properties was not considered.

Li *et al* (2011), in their work, fabricated a nanocomposites whose dielectric constant and electric conductivity was found to be strongly dependent on frequency and temperature. In their work, an

extremely large value of ε = 492 was achieved by adding 3 per hour GN (Nanographite) loading. However, this hybrid is unsuitable for energy storage applications due to its extremely large dielectric loss resulting from the formation of GN network. Ching *et al,* (2012), worked on LDPE material reinforced with varying composition of nanoalumina particles treated with silanes which were prepared for mechanical and morphology studies. Results gotten from the work revealed that the IR spectrum from FTIR analysis indicated that there was no chemical reaction between LDPE matrix and alumina particles and that the incorporation of 1wt% of nanoalumina particles caused agglomeration and uneven distribution of the particles throughout the LDPE matrix.

The work of Khumalo *et al*(2010), was devoted to determine the effects of synthetic boehmite alumina (BA) on the morphology, thermal, thermo-oxidative and rheological behavior of polyethylenes (PEs). It was found that BA at nanoscale dispersed in both LDPE and HDPE without any surface treatment and additional polymeric compatibilizer. Also BA practically did not influence the thermal (melting and crystallization) and rheological properties of the parent PEs. On the other hand, BA worked as a powerful thermo-oxidative stabilizer for LDPE, and especially for HDPE nanocomposites. Jenney (2010) worked on characterization of mechanical, morphological and thermal properties of LDPE nanocomposites using alumina nanoparticles as fillers. The mechanical properties were improved but there was no significant difference in its thermal stability. Christopher *et al* (2010), worked on Polyamideimide-alumina nanocomposites for high temperatures. Addition of alumina nanoparticles increased the real permittivity of the nanocomposites due to a combination of the nanoparticles higher permittivity and the interfacial region between the particles and the matrix.

Viscoelastic behaviour and fracture toughness of linear-low-density polyethylene reinforced with synthetic boehmite alumina nanoparticles was examined by Pedrazzoli *et al* (2013). The presence of Boehmite-alumina slightly enhanced the resistance to thermo-oxidative degradation of the LLDPE but surprisingly, the melt viscosity was reduced by the nanofillers matrix. Carmen e*t al* (2015), worked on Novel Nanocomposites of Poly(lauryl methacrylate)-Grafted Al_2O_3 Nanoparticles in LDPE. The dielectric measurements showed a decrease in tan δ values for LDPE nanoparticles modified by poly(lauryl methacrylate), as compared to the nanocomposites containing unmodified NP, thus indicating an improved interphase between the nanoparticles and LDPE. Chen *et al* (2009) also on Conduction in Linear-low Density Polyethylene Nanodielectric Materials studied the electrical conduction processes in linear low density polyethylene (LLDPE) filled with nano alumina particles. They found that the conduction current shows a minimum at 1% w.w. concentration nano alumina particles. Finally, Glulio *et al* (2010) examined the Effect of various alumina nano-fillers on the thermal and mechanical behaviour of low-density polyethylene–Al_2O_3 composites. The thermal and mechanical properties of the composites were improved and the composites also showed a higher thermo-oxidative stability with respect to neat LDPE.

1.6 Theoretical Background and Basic Principles on Nanocomposites

1.6.1 Polyethylene

Polyethylene is a thermoplastic polymeric material. It is highly used in consumer products and over 60 million tons of the materials are produced worldwide every year. Polyethylene is produced from ethylene gas. Polyethylene became very popular as power cable insulation when it was firstly introduced in 1960s, due to its low cost, better electrical properties compared to paper-oil insulation, processability, moisture and chemical resistance, and low temperature

flexibility (Andrews et al, 2006). There are several types of PE, usually classified according to their density into low (LDPE), medium (MDPE), and high-density (HDPE) PE. LDPE is most commonly used in power cables, because it has a low relative permittivity of about 2.3 and very low dielectric loss tangent due to the absence of any permanent dipolar groups. The operating temperature of LDPE is restricted to 70°C because of its thermoplastic nature and it starts to soften at 80-90°C and melts at 110-115°C (Tony and David, 2005).

Polyethylene exhibits three types of unit cells—orthorhombic, monoclinic, and hexagonal—all of which are relatively simple compared to other polyolefins and to polymers in general. The orthorhombic unit cell is by far the most common; for all practical purposes it may be considered to be the only one present in commercial samples (Andrews, 2000).

LDPE is defined by a density range of 0.910- 0.940 g/cm³. It is unreactive at room temperatures, except by strong oxidizing agents, and some solvent causes welling. It has more branching, so its intermolecular forces are weak, with lower tensile strength, and its higher resilience. Also, since its molecules are less tightly packed and less crystalline because of the side branches, its density is lower. Low density polyethylene is considered as one of the commercially important thermoplastics, especially for their low density, good processability, and easier mouldability for a wide range of applications. LDPE is more flexible than HDPE, which makes it a good choice for prosthetic devices (Andrews, 2000).

1.6.2 Properties of nanocomposites

Many material properties affect the decreasing behaviour of the grain size within the material. This section summarizes some of the most important properties of nanophase materials. These properties include catalytic, electronic, mechanical, transport and magnetic properties of

nanophase materials. These properties make nanophase materials attractive to study both for fundamental aspects as well as for potential novel application (Tarja, 1999).

1.6.2.1 Catalytic properties

Catalytic properties studies are predominantly based on single crystal surfaces of metal in vacuum. There is very little information on catalytic processes involving oxides (Tarja, 1999).. Catalytic reactions involve the following general surface chemical steps

i. Adsorption of the reactant molecules at surface sites

ii. Bond breaking of the adsorbates

iii. Rearrangement of the adsorbed reaction intermediates

iv. Desorption of the molecules (Tarja, 1999).

1.6.2.2 Electronic properties

The wave functions of electrons and holes are confined to the particle volume for small particles. If the particle size becomes comparable to or smaller than the de Broglie wavelength of the charge carriers, the confinement increases the energy required for creating an electron/hole pair. This increase shifts the absorption/luminescence spectra towards shorter wavelengths (so called "blue shift")(Tarja, 1999). In direct gap semiconductors, the band gap increases with decreasing particle size, and the excited electronic states become discrete with high oscillator strength. The optical absorption spectrum of γ-Fe_2O_3 is red shifted, which can be explained by the lattice strain in small particles (Giannelis *et al*, 1994). In a polymer matrix γ-Fe_2O_3 shows optical transparency in the visible range.

1.6.2.3 Mechanical properties

Grain size reduction usually yields improvements in strength and hardness in plastic deformation. Grain size reduction increases the strength and hardness, due to new grain boundaries, which act as effective barriers to dislocation motion. However, it may affect other mechanical properties negatively, such as creep rate and ductility. On the other hand, in materials that are conventionally quite strong but very brittle, such as intermetallic compounds and ceramics, enhanced ductility from grain size reduction, through the increased grain boundary sliding, can be considered favorable (Siegel and Fougere, 1994, Siegel and Fougere, 1995).

1.6.2.4 Magnetic properties

In order to reduce the large magnetostatic of single domain particles, a crystal will be broken up into a number of domains. Dipolar energy can be reduced by dividing a magnetic specimen into uniformly magnetized domains of macroscopic size, whose magnetization vectors point in wide and different directions. Such subdivision is paid for in exchange of energy, for the spins near the boundary of a domain will experience unfavorable exchange interactions with the nearby spins in the neighboring domain. Only the spins near the boundaries will have higher exchange energies but the magnetic dipolar energy drops for every spin when domains are formed (Ashcroft and Mermin, 1976). When the crystal size is reduced below a critical value L_c of a few hundred Ångströms a single crystal will become a single domain. In the single domain particles (SD) it is not energetically favorable to get magnetization reversed in the particle so no walls are formed.

The extrinsic magnetic properties of particles depend strongly upon their shape and size. This result was obtained when magnetostatic, exchange and domain wall energies were considered. However, interactions between particles also affect the critical size. Among magnetic properties

coercivity H_c shows a marked size effect. Saturation magnetization on the other hand is not dependent on the particle size (Wohlfarth, 1980).

CHAPTER TWO

LITERATURE REVIEW

2.1 Introduction

The field of nanocomposites or nanotechnology is a promising and advancing field because it has found application in advancing technology. A wide range of clays and polymers have been used successfully to synthesis a polymer nanocomposites. This review will be centered on the specific field under study LDPE/clay nanocomposites with emphasis on the general mode of preparation, characterization of nanocomposites materials and relevant areas of application as employed by other researchers.

2.2 Nanocomposites Synthesis

To prepare any nanocomposites, many methods have been employed previously. One successful method to prepare polymer/layered silicate nanocomposites is to intercalate polymers into silicate galleries. In general, intercalation of polymer chains into the silicate galleries is done by using one of the following processing techniques according to (Quang and Donald, 2006);

2.2.1 In-situ polymerization method

In this method, layered silicate is swollen within the liquid monomer solution so that the formation of polymer can occur between and around the intercalated layers. The polymerization can be initiated either by the incorporation of curing agent, initiator or by increasing the temperature if it is sufficiently reactive.

2.2.2 Solution blending method

This method is based on a solvent system in which the polymer is soluble and the silicate layers are swellable. The layered silicate is first swollen in a solvent. When the polymer and layered

silicate solutions are mixed, the polymer chains intercalate and displace the solvent within the interlayer of the silicate. Upon solvent removal, the intercalated structure remains, resulting in nanocomposites. Using this method, intercalation only occurs for certain polymer/solvent pairs. The disadvantages of this method are the use of environmentally unfriendly and economically prohibitive organic solvents.

2.2.3 Melt intercalation method

The melt intercalation technique has become the standard for polymer/layered silicate nanocomposites and is also quite compatible with the industrial techniques. In this method polymer and modified layered silicate mixture are blended in the molten state under shear. The polymer chains reptate form the molten mass into the silicate galleries to form either intercalated or delaminated nanocomposites.

2.2.4 Latex compounding method

This method is also a promising method in mostly rubber/layered silicate nanocomposites. Latex compounding technique starts with dispersing layered silicates in water which acts as a swelling agent owing to hydration of the intergallery cations. Rubber latex is then added and mixed for a period of time, with the dispersion of layered silicate in water followed by coagulation.

Sonication, adsorption via sonication, extrusion and spin casting technique are other methods that have also been reported in literatures in recent times. However, since solvent casting or melt intercalation appears to be the easiest and the one that is less time consuming of all the method for the synthesis of polymer nanocomposites, it is the most common method usually employed.

2.3 Modification of Clay Layers

The preparation of polymer/clay nanocomposites with good dispersion of clay layers within the polymer matrix is not easily achievable by physical mixing of polymer and clay particles. It is not possible to disperse nanoparticles in most polymers due to the high face to face stacking of layers in agglomerated tactoids and their intrinsic hydrophilic nature which make them incompatible with hydrophobic polymers. Only a few hydrophilic polymers such as poly (ethylene oxide) and poly (vinyl alcohol) can be miscible with clay nanolayers (Pavildou and Papaspyrides, 2008). As a result of the intrinsic incompatibility of hydrophilic clay layers with hydrophobic polymer chains, the dispersion of clay nanoparticles within polymer matrix could be hindered and the resulting material may also be of weak interfacial interactions.

Since incompatibility and weak interfacial interactions hinders the exfoliation and preparation of dispersed stable nanocomposite with improved properties, it is therefore necessary to modify the clay layers with hydrophobic agents in order to render it more compatible with polymer chains.

The surface modification of clay layers can be achieved through a cation exchange process by the replacement of sodium and calcium cations present in the interlayer space or clay galleries by alkylammonium or alkylphosphonium (onium) cations (Ahmad et al., 2009). In addition to the surface modification and increasing the hydrophobic nature of clay layers, the insertion of alkylammonium or alkylphosphonium cations into the galleries causes some degree of increase in the interlayer spacing. promotes the intercalation of polymer chains into the galleries during nanocomposite preparation (Chigwada et al., 2006).

Also the alkylammonium or alkylphosphonium cations can provide functional groups which interact with polymer chains or initiate the polymerization and therefore increase the interfacial interactions.

2.4 Types of Nanocomposite Structures

The incorporation of a few weight percent of modified layered silicates which are properly dispersed in the polymer matrix can result in very high surface areas for polymer/layered silicate interactions, as compared to the conventional polymer/filler composites. According to the strength of the interfacial between polymer matrix and layered silicate four type of polymer/clay composites can be produced (Cicek, 2008).

2.4.1 Conventional composites

In a conventional polymer composite, layered silicate acts as conventional, micron sized fillers such as carbon black clusters or other inorganic fillers.

2.4.2 Intercalated nanocomposites

Intercalated nanocomposites are formed by the insertion of a rubber chains between the unaltered silicate layers, maintaining their regular alternation of galleries and laminas.

2.4.3 Exfoliated nanocomposites

In exfoliated nanocomposites the individual layers of the nanoclay are totally delaminated and are usually dispersed in the matrix. The ordered structure of layered silicate is lost and the average distances between the exfoliated layers depend on clay loading.

2.4.4 Intermediate nanocomposites

Rubber-clay nanocomposites which are partially intercalated and partially exfoliated are an intermediate type of nanocomposites.

2.5 Electrical Properties of Polymers

2.5.1 Polymer as non-conductive materials

The electrons in polymers are fixed together by σ-bonds, as such there are no electrons free to carry an electric current. Hence, solid, saturated polymers are characteristically electrical insulators. This makes it possible for it to retain for a long time any electrostatic charges they acquire. Since charges are deposited by mere contact with different materials, the charged condition is frequently encountered with particles made from polymers. Notably important, although contact charges represent only a slight imbalance of charge compared with the total amounts of positive and negative charge present in matter, they can nevertheless give rise to electric field which is high enough to cause sparking in air (Tony and David, 2005).

2.5.2 Polymer as conductive materials

It was expected that π −bonding in a conjugated chain would produce bonds of equal length, with p_z orbital of each bond overlapping with those of both of his neighbours along the chain. This uniform orbital overlap would form a π −electron wave function stretching over the whole polymer backbone. This also leads to delocalization of electron which are free to move along the polymer backbone. Polymer is described in this case as a one-dimensional metal with a half filled conduction band. But localisation of electrons in the double or triple bond which characterise the conjugated polymers, however lowers the overall energy of the electron system. The concomitant increase in the energy gap in the electron has a profound effect on the properties of the polymers, with the presence of the energy gap turning into a semiconductor. Therefore, the possibility of exciting π −electrons out of the localised π −bonds by the absorption of visible photons gives rise to electrical conduction. (Tony and David, 2005)

2.6 Dielectric Properties of Insulation Materials

2.6.1 Polarization of dielectric materials

When a uniform static electric field E is applied on a plate capacitor with vacuum medium between the electrodes, according to Coulomb's law,

$$Q = \varepsilon_o E \qquad 2.1$$

Where ε_o is the free space permittivity with the value 8.85×10^{-12} F/m. The capacitance of the vacuum plate capacitor

$$C_o = \frac{Q}{V} \qquad 2.2$$

If a dielectric material is inserted between the electrodes, as shown in Figure 2.1 with solid line connection of DC voltage application, the material will respond to the applied electric field by redistributing its component charges to some extent. Positive charges will be attracted towards the negative electrode and vice versa. This effect is called polarization of the material (Tony and David.,2005).

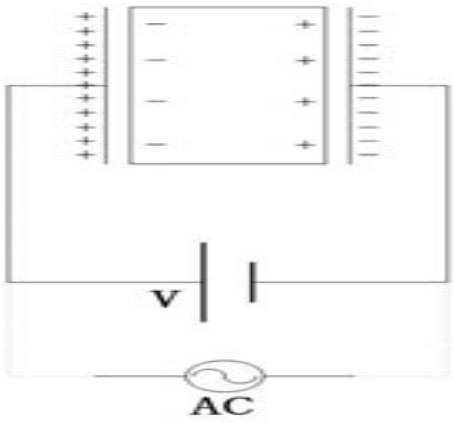

Figure 2.1 Polarization of dielectric material between plate electrodes

If the material is isotropic, certain amount of dipoles will be produced, aligning in the field direction inside the material. Thus, the polarization P is defined as a vector quantity of the magnitude and direction of the electric moment per unit volume in the material by the applied field. The polarization with bound charges makes more charge stored on the electrodes and, therefore, the capacitance after inserting the dielectric medium is increased. The ratio of the increased capacitance C to the vacuum capacitance C_0 used to be called dielectric constant and now is more scientifically named as real part relative permittivity ε ′ ,

$$\varepsilon = \frac{C}{C_0} = \frac{Q+P}{Q} = \frac{(\varepsilon_0 E+P)}{\varepsilon_0 E} = 1 + \frac{P}{\varepsilon_0 E} = 1 + \chi \qquad 2.3$$

Where χ is the susceptibility of the material, ε describes the ability of polarization that occurs in the material and is an important property of dielectric materials, depending on the frequency of the field applied, humidity and temperature.

In electromagnetism, the electric displacement field D represents how an electric field E influences the organization of electrical charges in a given medium, including charge migration and electric dipole reorientation. With the above Equation 2-3 the electric displacement D in the material may be obtained by rearranging it as

$$D = \varepsilon_0 \varepsilon E = \varepsilon_0 E + P \qquad 2.4$$

This is the fundamental electric field equation that applies at any point in an isotropic medium.

In this context, the maximum polarization, corresponding to the highest observable relative permittivity, will be realised only when sufficient time is allowed after the application of an electric field. The observed permittivity is static permittivity (dielectric constant) ε if ample time is allowed. On the other hand, if the polarization is measured immediately after the field is applied, allowing no time for dipole orientation, the instantaneous relative permittivity ε_∞ will be observed. Between these two extremes of time scale there is a dispersion, which could be

examined by applying an alternating electric field E with magnitude $_0E$ and angular frequency ω,

across a dielectric material$E = E_o cos\omega t$. This will produce polarization, which alternates in direction, and if the frequency is high enough, the orientation of any dipoles will inevitably lag behind the applied field. As shown in Figure 2.2, the lag of polarization can be expressed as a phase lag δ in the electric displacement:

$$D = D_o \cos(wt - \delta) \quad 2.5$$

$$D = D_o cos\omega t cos\delta + D_o sin\omega t sin\delta \quad 2.6$$

which leads to the definition of two relative permittivities

$$\varepsilon' = \frac{Dcos\delta}{\varepsilon_o E_o} \; and \; \varepsilon'' = \frac{Dsin\delta}{\varepsilon_o E_o} \quad 2.7$$

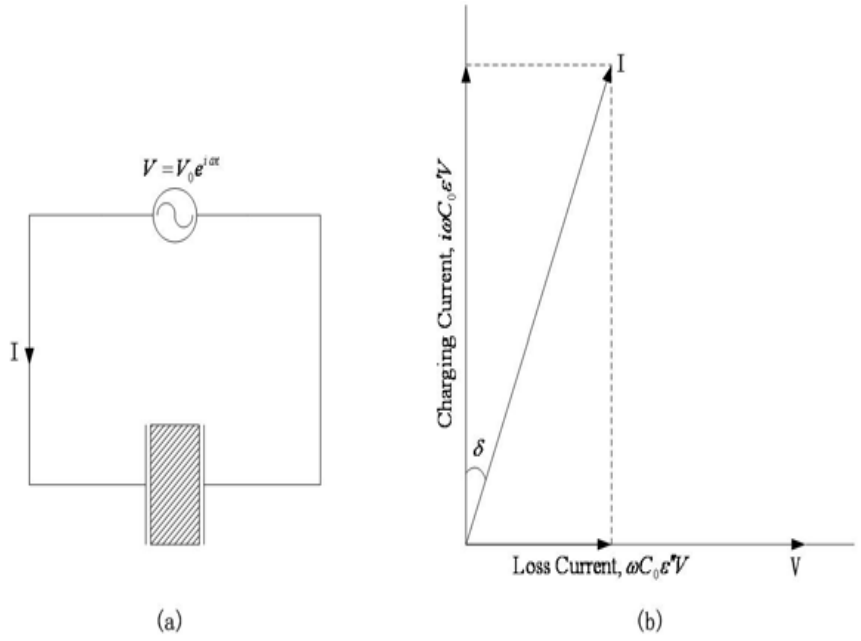

Figure 2.2: AC losses in a dielectric: (a) circuit diagram, (b) Argand diagram of complex current-voltage relationship (Tong liu, 2010)

At different frequencies, these two quantities are dependent on the lag angle δ , which represents the molecular behaviour for different dielectrics. They are combined into a

complex relative permittivity $\varepsilon^* = (\omega)$ for dielectric spectroscopy studies.

$$\varepsilon^*(\omega) = \varepsilon'(\omega) + i\varepsilon''(\omega) \qquad 2.8$$

There are a number of different dielectric polarization mechanisms at the molecular or microscopic level, connected to the way a studied medium reacts to the applied field.

Each dielectric mechanism is centred around its characteristic frequency, which is the reciprocal of the characteristic time of the process. In general, dielectric polarization mechanisms can be divided into relaxation and resonance processes. Dielectric relaxation is the momentary delay in the dielectric constant of a material. This is usually caused by the delay in molecular polarization with respect to a changing electric field in a dielectric medium. Dielectric relaxation in changing electric fields could be considered analogous to hysteresis in changing magnetic fields. Relaxation in general is a delay or lag in the response of a linear system, and therefore dielectric relaxation is measured relative to the expected linear steady state (equilibrium) dielectric values.

2.6.2 Debye relaxation and modifications

The dielectric relaxation for an ideal, non-interacting population of dipoles can be described by the classic Debye relaxation (semicircular arc rule). This is usually expressed in terms of the complex permittivity ε^* of a medium as a function of angle frequency ω

$$\varepsilon^*(\omega) = \varepsilon_\infty + \frac{\Delta\varepsilon}{1+i\omega\tau} \qquad 2.9$$

Where ε_∞ is the permittivity at the high frequency limit, $\Delta\varepsilon = \varepsilon_s - \varepsilon_\infty$, ε_s the static, low frequency permittivity, and τ the characteristic relaxation time of the medium. In most cases, the complex plane often deviates from a semicircle, resulting from the relaxation time effect. Havriliak-Negami relaxation (Havriliak and Negami, 1966,1967), an empirical modification of Debye relaxation is then proposed due to the asymmetry and broadness of dielectric dispersion

curves. The model is used to describe the dielectric relaxation of polymers by adding two exponents to the Debye equation:

$$\varepsilon^*(\omega) = \varepsilon_\infty + \frac{\Delta\varepsilon}{(1+(i\omega\tau)^\alpha)^\beta} \quad 2.10$$

Where exponents α and β describe the asymmetry and broadness of the corresponding spectra. Cole-Cole equation is a special case of Havriliak-Negami relaxation in which the parameter β equals to unity:

$$\varepsilon^*(\omega) = \varepsilon_\infty + \frac{\Delta\varepsilon}{1+(i\omega\tau)^\alpha} \quad 2.11$$

That is when the relation peaks are symmetric (cole and cole, 1941),

Most polymers show dielectric relaxation patterns that can be accurately modeled by this equation. The Havriliak -Negami equation can be simplified to Davidson-Cole expression (Davidson and Cole, 1951) when the exponent $\alpha = 1$. It improved the fit with experiment by using a slightly different semi-empirical equation:

$$\varepsilon^*(\omega) = \varepsilon_\infty + \frac{\Delta\varepsilon}{(1+i\omega\tau)^\beta} \quad 2.12$$

2.6.3 Further theoretical predictions

The exact prediction of the effective dielectric constant of polymer/ceramic composites is particularly useful for the design of composite materials. Different theoretical models have been proposed for predicting the permittivity of several mixtures. Maxwell considered non-interacting spherical particles in a homogeneous dielectric medium. This was improved by Rayleigh who believed that the interaction of particles through a regular array:

$$\varepsilon_c = \varepsilon_p(1 + 3x\left(\frac{\varepsilon_f - \varepsilon_p}{2\varepsilon_p + \varepsilon_f}\right)) \quad 2.13$$

where ε_c, ε_f, ε_p are the permittivity of composites, fillers and matrix, respectively.x is the filler volume concentration.

The logarithmic mixing role where Lichtnecker considered the composite as a random mixture of nearly spherical inclusions (Ramajo *et al*, 2005, Cheng *et al* 2007, Kulek *et al* 2007 and Kota *et al* 2007)

$$log\varepsilon_c = xlog\varepsilon_f + (1-x)log\varepsilon_p \qquad 2.14$$

In practice, composite materials are always likely to have regions of nonuniformity due to random mixture and inclusions, and impurities may be present as a second phase. Effects on dielectric properties attributable to material discontinuities are usually called Maxwell-Wagner effects. Therefore, Maxwell–Garnett approximation is applicable to polymer composites embedded with inclusions in a continuum matrix. This can be expressed as:

$$\varepsilon_c = \varepsilon_p(1 + \frac{3xA}{1-xA}) \qquad 2.15$$

Where $A = \frac{\varepsilon_f - \varepsilon_p}{2\varepsilon_p + \varepsilon_f}$

2.7 Electronic Conduction in Polymers

Electrical conduction usually occurs through the movement of either electrons or ions. In each case, the conduction process has the basic equation:

$$\sigma = qn\mu \qquad 2.16$$

Where the conductivity σ is resolved into three factors, the charge q, the concentration n and the drift velocity μ of the carriers. The latter parameter describes the ease with which the charge species will move under the influence of the applied electric field E and is usually expressed as a velocity per unit field. Polyethylene, polytetraflouroethylene and polystyrene are among the best

insulators known, while polyacetylene can be obtained with a higher conductivity per unit than copper (Tony and David, 2005).

In polymers with chemically saturated structures, i.e σ −bonded backbones; it is very difficult to observe any electronic conductivity at all. If there were to be conductivity, it usually depends on the movement of adventitious ions. Consequently, any improvements in the quality of insulation are generally achieved by careful preparation and purification, in order to avoid as much as possible the presence of ionic impurities, including catalyst residues, products of oxidation and dissociable end group.

Electronic conduction is possible in polymers with chemically unsaturated (conjugated) structures, i.e π −bond backbones. To some extent the rigidity of the conjugated polymer backbones means that the two sets of properties are mutually exclusive.

2.8 Dielectric Spectroscopy Techniques

Dielectric spectroscopy also known as the impedance spectroscopy, measures the dielectric properties of a medium as a function of frequency. Dielectric spectroscopy can provide useful information relating the segmental mobility of a polymer by probing its dielectric properties. Its measurement is based on the interaction of an external field with the electric dipole moment of the sample, often expressed by permittivity (Dissado and Forthergil, 1992).

2.8.1 Bridge method

The most widely used way of determining the equivalent capacitance and resistance of a specimen is to use a type of Wheatstone bridge network to compare the unknown with standard components. The LCR impedance analyser mostly uses the bridge method. The common form for the measurement of dielectric materials is the Schering bridge, with which it is possible to

make very accurate measurements over the frequency range $10\ to\ 10^5 Hz$ (known as the audio frequency range).

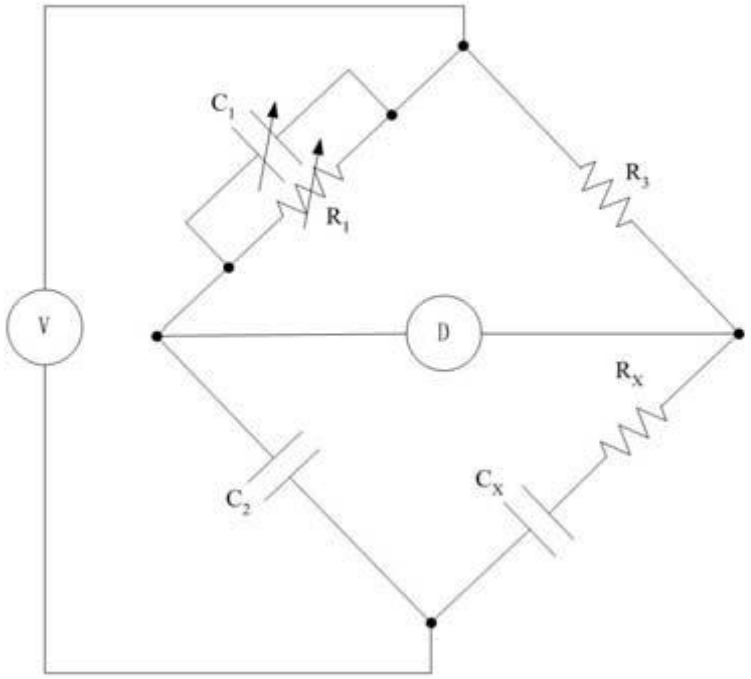

Figure 2.3; Circuit diagram of a conjugate Schering bridge (Tony and David, 2005)

The basic circuit for a practical form of the bridge is shown in figure 2.4. As the detector indicates a null deflection, it is said to be balanced, and we have a relation between the impedances of the arms as:

$$\frac{Z_1}{Z_2} = \frac{Z_3}{Z_4} \qquad 2.17$$

From the above, C_x and R_x can be calculated by

$$C_x = \frac{R_x \mathrm{x} C_1}{R_3} \text{ and } R_x = \frac{C_1 \mathrm{x} \mathrm{R}_3}{C_2}$$

Where C_2 andR_3 are fixed-value standard capacitor and resistor. When the angular frequency ω is determined, the loss tangent of the dielectric sample can be obtained by

$$tan\delta = \frac{1}{\omega R_x C_x} \qquad 2.18$$

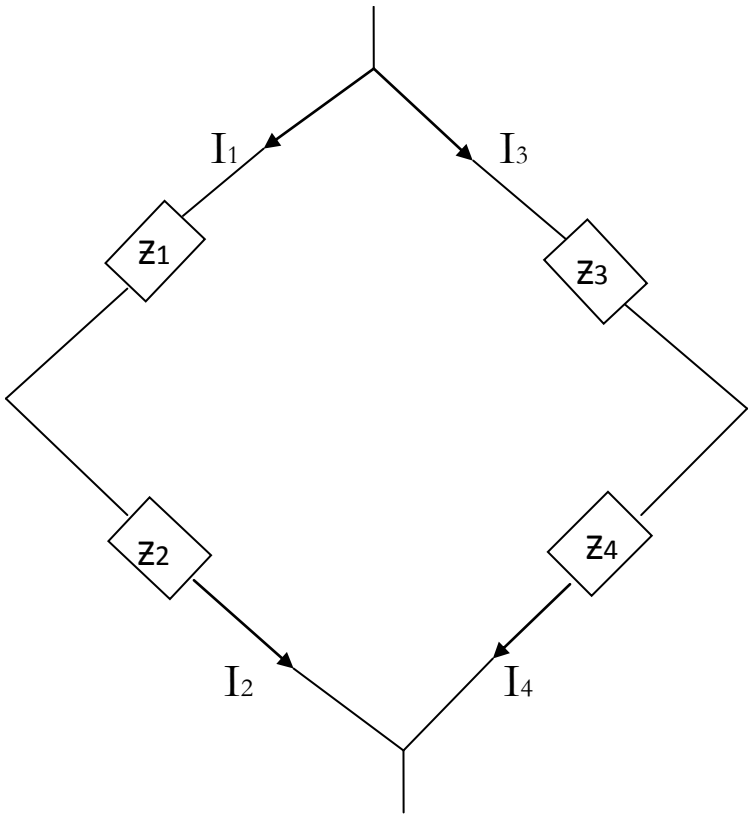

Fig 2.4: Basic circuit for a practical form of the bridge

The accuracy of an audio-frequency bridge depends on the effect of stray impedances which couple various current sources of the bridge with unknown amount, depending on the component settings and the position of operator. To eliminate this problem, extra electric components are used to form Wagner earth circuit as follows: the bridge is first balanced as normal, and then detector connected from one bridge corner to earth and the wagner circuit adjusted to give another null. This creates a disturbance until the bridge is balanced and the detector terminals are at earth potential. Under this condition, earth screens can be used around all bridge components, and a guard electrode can be used in the simple cell. This can give great precision with a Schering bridge over all its working range.

2.8.2 Frequency response analyser method

The frequency response analyzer, also called impedance analyzer, is an instrument for studying the frequency response of all kinds of materials. In principle, the fig 2.6, the frequency response analyser has two main parts: a generator which provides a digitally-synthesised alternating voltage $V_o cos\omega t$ over a range of frequency, and a correlator which measures the in-phase and quadrature component of any input signal with respect to the output of its generator.

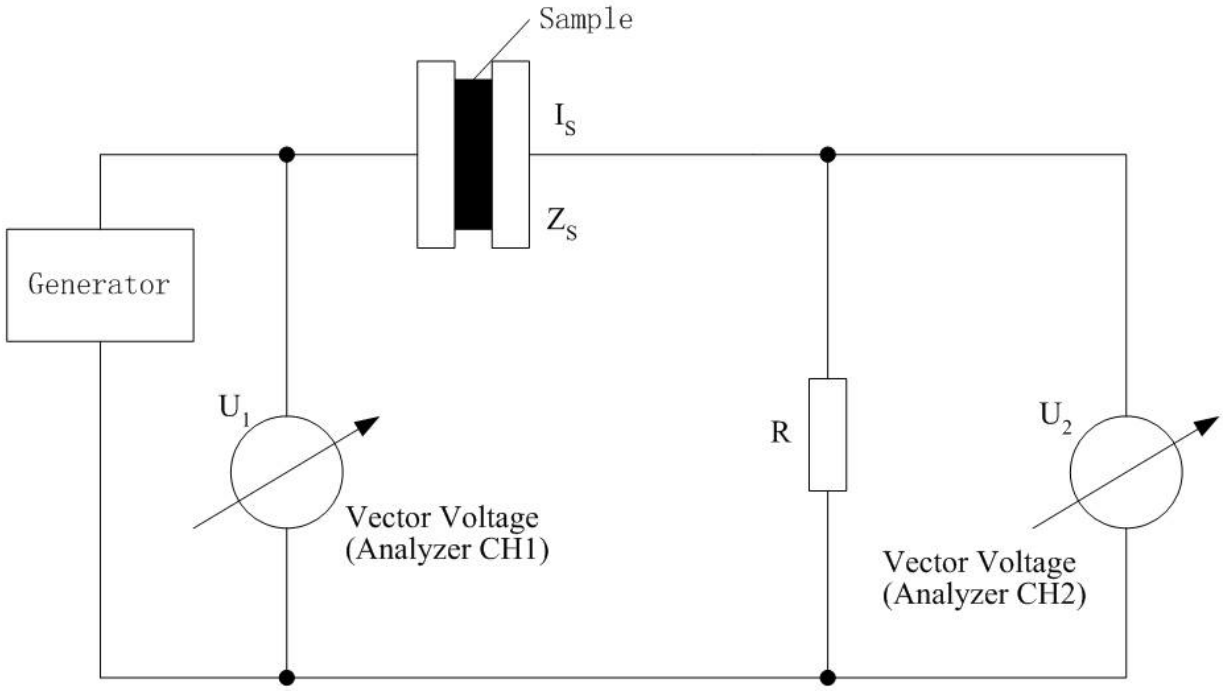

Figure 2.5 Schematic of frequency response analyzer (Tong liu, 2010)

The complex relative permittivity can be then calculated by

$$\varepsilon^* = \frac{1}{i\omega Z_S(\omega) C_O} \qquad 2.19$$

provided the geometric capacitance of the dielectric sample is known (James *et al*, 1999). The correlator works by multiplying the input signal by cosine and sine reference signals derived

directly from the generator and further integrating these products over certain frequency range. By this integration, reduces the noise level

2.9 Electrical Aging

Electrical aging is a gradual degradation process leading to destructive breakdown of a material. This happens when an insulating material is subjected to continuous electrical stress, the material will be in a non-equilibrium state and its properties will change with time. Under this condition, the material is said to undergo electrical aging. Generally, the lifetime of an electrically stressed material depends on the magnitude of the electric stress applied to the material and the length of the time it has been subjected to such a stress. This implies that the lifetime of a material depends mainly on the electrical contacts, which control carrier injection, and the kind and concentration of carrier traps, which control the degradation process. Electrical aging is always an important problem of concern to industry (Kwan,2004). The general features of insulating materials are:

i. Carrier mobility is low, usually lower than 10-1cm2V-1 s-1.

ii. Dielectric relaxation time is much greater than carrier lifetime.

iii. The energy band gap is large, generally larger than 4 eV.

iv. The localized gap state concentration is much larger than the thermal equilibrium carrier concentration.

v. The mean free path is small, usually of the order of several molecular radii (5–20Å). Electrons may be injected into the insulator by a thermionic emission process or by an electron tunneling process due to applied field. These injected electrons will quickly become trapped after a few scatterings because of the small mean free path (Kwan, 2004)

Electron trapping will result in the following two important phenomena:

i. The trapped electrons will form a negatively charged homo–space charge near the electron-injecting contact (cathode) and hence create an internal field F_i opposite to the applied field, reducing the effective field for and rate of electron injection. This space charge also enhances the field toward the anode and may switch on hole injection.

ii. In the transition from an upper to a lower energy state due to trapping (or recombination), an energy equal to the energy difference between the two states will be evolved, which is mainly nonradioactive for non-crystalline insulating materials. The energy evolved at each trapping or recombination event is of the order of 3–4eV or greater for deep traps and recombination centers. (kwan, 2004)

This dissipation of the energy evolved due to nonradioactive transition of electron trapping or recombination in causing damage to the material structure.

2.10 Electrical Discharge

An electrical discharge is a process by which atoms or molecules become electrically charged due to ionization by avalanches of hot carriers, mostly starting in the medium of gas state. Electrical discharges that do not bridge the electrodes or any pair of electrical contacts in an electrical system are called partial discharges.

In fact, all partial discharges involve gas discharges (Kreuger, 1965).

In general, partial discharges can be classified into four types:

i. Corona discharges: These generally refer to discharges occurring in the vicinity of a sharp point or edge of a metallic contact, or in the vicinity of a conducting particle whose surrounding field is extremely high due to divergent or inhomogeneous field distribution.

ii. Surface discharges: These discharges occur on the surface of a dielectric material,

iii. Internal discharges: These discharges occur in inclusions or cavities originally existing in a dielectric material, or in low density domains or channels created due to electrical stressing at high fields

iv. Electrical treeing: Electrical treeing may be considered a combination of corona and internal discharges.

All electrical discharges are detrimental to dielectric materials. They may cause permanent changes in chemical structure or in constituent elements of the material's molecules

2.11 Dielectric Breakdown

When electrical insulators are subjected to a potential difference of increasing magnitude, a point is attained at which they physically break down and begin to conduct electricity. The dielectric strength of a sample is the voltage gradient at which this failure occurs. The (dielectric) breakdown voltage is the potential difference at which dielectric failure occurs under specified conditions. In practice, dielectric strength or breakdown voltage is determined by applying an electric field across an insulator and ramping it at a fixed rate until the sample fails (Andrew, 2000). Failure is defined as puncturing of the sample with subsequent conduction of electricity. Test specimens can take many forms, ranging from end use products to sheet and film molded specifically for purposes of testing.

Usually when non-symmetrical products are to be tested, standard electrode positions are adopted. Electrodes are preferably metal plates of a standard shape, size, and surface finish, but other types may be employed as conditions may warrant. One of the electrodes (normally the larger if there is a difference in size) is grounded, and the other is attached to a controllable source of alternating voltage. The root mean square (rms) voltage is increased according to one of three general methods. In method 1, the ‘‘short-time test,’’ the applied voltage is ramped

steadily from zero at a constant rate ranging from 100 to 5000 V/sec. The ramp rate is chosen such that failure occurs within 10–20 sec of the start of the test. Method 2, the ‘‘step-by-step test,’’ calls for the incremental increase of voltage as a function of time, the increment and interval between steps being constant. Increments may be in the range of 0.25–10 kV, with a typical time interval of 60 sec. The starting voltage is selected such that failure occurs within 4–10 steps. In method C, the ‘‘slow rate of rise test,’’ the applied voltage is ramped steadily at a constant rate, starting from a predetermined voltage similar to that used in method 3. The voltage is increased at a rate that approximates the average rate of increase used in method B. Breakdown should occur after a minimum of 120 sec, at a voltage not to exceed 1.5 times the initial value. Failure is deemed to occur when there is an abrupt increase in measured current, normally accompanied by a physical rupturing of the specimen that is frequently audible. In the case of the step-by-step test, the breakdown voltage is taken to be that of the last complete time interval before failure. For each sample a minimum of five specimens are run and the average breakdown value is reported. The dielectric strength is the breakdown voltage divided by the thickness of the specimen.

The coefficient of variation reported for a single operator is usually less than 9%. When different operators using different sets of equipment analyze a given material, the single-operator coefficient of variation is approachable if all the experimental variables are rigorously controlled (Andrews, 2000).

2.12 Measuring Techniques

2.12.1 Fourier-transform infrared (FTIR) spectroscopy

Infrared (IR) refers to that part of the electromagnetic spectrum between the visible and microwave region. Fourier-transform infrared (FTIR) spectroscopy is based on the idea of the

interference of radiation between two beams to yield an interferogram. The interferogram is a signal produced as a function of the change of path-length between the two beams. The two domains of distance and frequency are inter-convertible by the mathematical method of Fourier-transformation (Barbara, 2004).

The basic idea is that the radiation emerging from the source is passed through an interferometer to the sample before reaching a detector. Upon amplification of the signal, in which high-frequency contributions have been eliminated by a filter, the data are converted to digital form by an analog-to-digital converter and transferred to the computer for Fourier-transformation

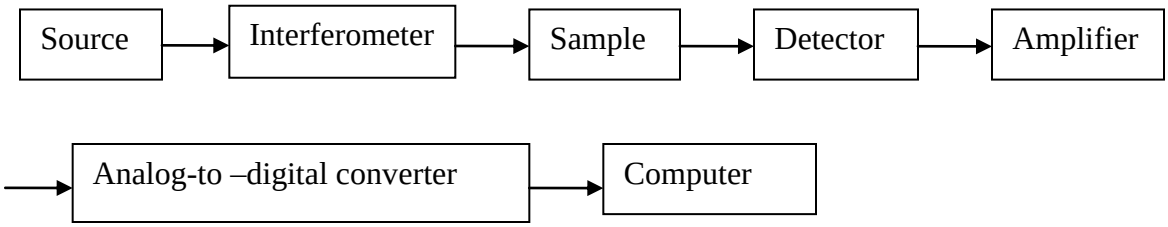

Fig 2.6: Basic components of an FTIR spectrometer.

FTIR spectrometers use a Globar or Nernst source for the mid-infrared region. If the far-infrared region is to be examined, then a high-pressure mercury lamp can be used. For the near-infrared, tungsten–halogen lamps are used as sources. There are two commonly used detectors employed for the mid-infrared region. The normal detector for routine use is a pyroelectric device incorporating deuterium. For more sensitive work, mercury cadmium telluride (MCT) can be used, but this has to be cooled to liquid nitrogen temperatures. In the far-infrared region, germanium or indium–antimony detectors are employed, operating at liquid helium temperatures. For the near-infrared region, the detectors used are generally lead sulfide photoconductors tryglycine sulfate (DTGS) in a temperature-resistant alkali halide window.

Band positions in IR spectra are usually presented as wavenumbers ($\bar{v}$) which unit is the reciprocal of centimeter (cm^{-1}). This unit is proportional to the energy of vibration as modern instruments are linear in reciprocal centimeters. Also band intensities can be expressed either as transmittance (T) or absorbance (A). Transmittance is the ratio of the radiant power incident on the sample while absorbance is the logarithm to the base 10 of the reciprocal of the transmittance (Robert *et al*.,2005).

There are two types of molecular vibration; stretching and bending. A stretching vibration is a rhythmical movement along the bond axis such that the interatomic distance is increasing or decreasing while a bending vibration consists of a change in bond angle between bonds with common atomsor the movement of a group of atoms with respect to the remainder of the molecule without movement of the atoms in the group with respect to one another (Robert *et al*, 2005)

The essential equations for a Fourier-transformation relating the intensity falling on the detector, $I(\delta)$, to the spectral power density at a particular wavenumber, $\bar{v}$, given by $B(\bar{v})$, are as follows

$$I(\delta) = \int_0^{+\infty} B(\bar{v})\cos(2\pi\overline{v\delta})d\bar{v} \qquad 2.20$$

which is one half of a cosine Fourier-transform pair, with the other being:

$$B(\bar{v}) = \int_0^{+\infty} I(\delta)\cos(2\pi\overline{v\delta})d\delta \qquad 2.21$$

2.12.2 Scanning electron microscopy

Scanning electron microscopy (SEM) is usually used to determine particle size and distribution and to examine fracture surfaces. The SEM consists of an electron gun producing a source of electrons at an energy range of 1-40keV. Electron lenses reduce the diameter of the electron beam and place a small focused beam on the specimen. The electron beam interacts with the

near-surface region of the specimen to a depth of about 1μm and generates signals used to form an image. The smaller the beam size, the better the resolution of the image (Oliver, 1974). The Phenom ProX SEM used for this study is capable of differentiating particle detail as small as 1 nm depending on elemental contrast and other parameters. The smaller the beam size, however, the less current available to form a clear picture. Operating the SEM requires fine tuning to optimize picture quality with resolution. SEM is run under a vacuum to minimize beam interactions with gas molecules which would retard resolution (Greene *et al*, 2004). Non-conductive specimens, such as most polymers, often suffer from variations in surface potential which introduce astigmatism, instabilities, and false x-ray signals. Charging, a condition during which charge accumulates on the surface of a non-conducting specimen causing excessive brightness, often occurs making it difficult to obtain quality images. Sputter coating non-conductive samples with a fine gold layer is often required to avoid these issues (Goldstein *et al*.,1992)

2.12.3 X-ray diffraction (XRD)

In X-Ray diffraction, electromagnetic radiations are treated as waves. The discovery of X-rays in 1895 enabled scientists to probe crystalline structure at the atomic level. X-ray diffraction has been in use in two main areas, for the fingerprint characterization of crystalline materials and the determination of their structure. Each crystalline solid has its unique characteristic X-ray powder pattern which may be used as a "fingerprint" for its identification. Once the material has been identified, X-ray crystallography may be used to determine its crystalline structure, i.e. how the atoms are arranged together in the crystalline state and what the interatomic distance and angle are etc. X-ray diffraction is one of the most important characterization tools used in solid state physics and materials science. The size and the shape of the unit cell for any compound can be

determined mostly by easily using X-ray diffraction. Usually a crystal consists of a periodic arrangement of the unit cell into a lattice. The unit cell can contain a single atom or atoms in a fixed arrangement. Crystals consist of planes of atoms that are spaced a distance d apart, but can be resolved into many atomic planes, each with a different *d* spacing *a*, *b* and *c* (length) and α, β and γ angles between *a*, *b* and *c* are lattice constants or parameters which can be determined by XRD (Inouye and Kirschner, 1997).

X-ray diffraction provides most definitive structural information, interatomic distances and bond angles. It also provides information about structures we need to probe atomic distances which requires a probe wavelength of 0.1 nm. They are produced by bombarding a metal target (Cu, Mo usually) with a beam of electrons emitted from a hot filament (often tungsten). X-rays are produced whenever high-speed electrons collide with a metal target. A source of electrons – hot W filament, a high accelerating voltage between the cathode (W) and the anode and a metal target,(*Cu*, Al, Mo, Mg). The anode is a water-cooled block of Cu containing desired target metal. The incident beam will ionize electrons from the K-shell (1s) of the target atom and X-rays are emitted as the resultant vacancies are filled by electrons dropping down from the L (2P) or M (3p) levels. This gives rise to Ka and Kb lines (Inouye and Kirschner, 1997).

The patterns generated by from the sample may be used to confirm that you have made a known or unknown material by searching/matching using the ICDD data base. They have about 100,000 patterns on file. For a new material, you need to index the pattern. Unit cell, lattice parameters and symmetry, are also provided by the XRD as results (Inouye and Kirschner, 1997).

Plate 2.1: Showing A typical X-Ray Diffraction spectroscopy

2.12.4 Nanoindentation

Nanoindentation instrument provides a valid approach to investigate the mechanical characterizations of nanomaterials, such as the hardness, dislocation motion, and Young's modulus, which are required to design structural/functional elements in micro- and nanoscale devices (Zhi-Qiang *et al.*, 2010). Conventional indentation hardness tests are done based on the measurement of the size of a residual plastic impression in the specimen as a function of the indenter load. This provides a measure of the area of contact for a given indenter load. But in a nanoindentation test, the size of the residual impression is often only a few microns and this

makes it very difficult to obtain a direct measure using optical techniques. In nanoindentation testing, the depth of penetration beneath the specimen surface is measured as the load is applied to the indenter. The known geometry of the indenter then allows the size of the area of contact to be determined (Fischer-Cripps, 2004).

The elastic modulus and hardness values are obtained from experimental values of load and depth which are described along with the methods of applying necessary corrections to the data. Usually, methods of analysis rely on the assumption of an elastic–plastic loading followed by an elastic unloading—with no plastic deformation (or "reverse" plasticity) occurring during the unloading sequence. The indentation modulus is usually determined from the slope of the unloading curve at maximum load. Equation 2.1 shows that the indentation modulus (expressed as E^*) as a function of dP/dh and the area of contact (Zhi-Qiang, *et al*, 2010).

$$E^* = \frac{1}{2}\frac{\sqrt{\pi}}{\sqrt{A}}\frac{dP}{dh} \qquad 2.22$$

Where P is the applied load, and h is the depth for an elastic–plastic contact while $\frac{dP}{dh}$ is known as stiffness of the contact. The indentation hardness is calculated from the indentation load divided by the projected contact area.

$$H = \frac{P}{A} \qquad 2.23$$

The nanoindentation instrument should be insulated against temperature variation, vibration, and acoustic noise in normal laboratory conditions. A nanoindentation instrument has a limited range of displacement over which the indentation depth may be measured. It is therefore necessary to ensure that the full range of the depth measurement system is available for measuring penetration depth into the specimen and not used for bringing the indenter into contact with the surface from its initial parked position (Zhi-Qiang *et al*, 2010).

The relationship between force and elongation does not obey the Hooke's law, even at very low deformations. Thus the elastic constant of this region, which is the stress required to deform the sample by a given strain, usually decreases as a function of elongation. The elastic constant is variously referred to as the ''initial modulus,'' ''tensile modulus,'' ''Young's modulus,'' ''elastic modulus,'' or simply the ''modulus'' of the sample. The elastic modulus of a sample is a measure of its rigidity; the higher the modulus, the stiffer the sample. The value of elastic modulus is normally derived from the initial slope of the force versus elongation plot. The two most commonly used units are pounds per square inch (psi) and meganewtons per square meter (MN/m^2) [also known as megapascals (MPa)]; (1 psi= 0.0069 MN/m2; 1 MN/m2=145 psi). The local compressive strength of polyethylene is of more interest commercially than its bulk compressive modulus. Local compressive strength is normally referred to as ''hardness,'' ''microhardness'' or ''microindentation hardness'' (MH). Microhardness is important in terms of the retention of a good surface finish on molded articles. Microhardness can be determined from the dimensions of an indentation left by a stylus having a known profile applied to a specimen with a known force, Andrews (2000). The resulting value is quoted in terms of force per unit area or megapascal (MPa). The deformation caused by the indentor or needle involves rearrangement of the initial morphology and hence depends on structural parameters similar to those involved in the short range tensile deformation of polyethylene. The microhardness of a sample is thus strongly correlated with its tensile yield stress and elastic modulus and hence its degree of crystallinity. For a wide range of polyethylene samples, microhardness can be linearly related to degree of crystallinity, Andrews (2000). Hardness can also be determined from the penetration depth of a needle forced into a sample by a spring.

Generally, one potential concern regarding nanoindentation of polymer thin film samples is the impact of the substrate, that is, the glass slide on which the film lays, on the indentation results, this is a factor of the indentation depth and the sample thickness (Ciprari,2004)

2.12.5 LCR/Impedance analyser

The LCR meter obtains its name from the fact that the inductance, capacitance and resistance are denoted by L, C and R respectively. LCR Meters and specimen cells when readily available make it easy to perform impedance measurements on materials. It's a measuring instrument with a wide programmable frequency range which makes it an all important tool since the insulation properties can vary substantially with frequency.

A material is classified as "dielectric" if it has the ability to store energy when an external electric field is applied. A dielectric materials measurement can provide critical design parameter information for many electronics applications. For example, the loss of a cable insulator, the impedance of a substrate, or the frequency of a dielectric resonator can be related to its dielectric properties (Greg, 1997). The dielectric constant measurement which is also known as relative permittivity has the complex dielectric constant that consists of a real part (ε'), which represents the storage capability and an imaginary part ($\varepsilon^{''}$), which represents the dielectric loss. Dielectric constant measurements can be performed easier and faster by using the impedance analyser. The dielectric constant is therefore defined as the ratio of the capacitance of the material to the capacitance of air,

$$\varepsilon^{'} = \frac{C_x}{C_o} \qquad 2.24$$

where C_x = capacitance with a dielectric material and C_o = capacitance without material, or vacuum

Dissipation factor (D) is defined as the ratio of an insulating materials resistance to its capacitive reactance at a specified frequency. It measures the inefficiency or loss of the material, is always greater than 0, but usually much smaller than the dielectric constant. The dissipation factor measurements are an excellent means of quality control which can yield indication of contamination or deterioration (Ahmad, 2012).

CHAPTER THREE

3 MATERIALS AND METHODS

3.1 Introduction

This chapter describes the procedure used in the preparation of nanokaolin and nanoalum at different degrees of purity. It also describes two procedures involved in the synthesis of the alumina vis a vis acid leaching and thermal sintering methods. It also explains the doping technique which subsequently leads to the formation of the LDPE/alumina samples. The methods employed to carry out the morphological analysis; electrical measurement and mechanical analysis are also outlined.

3.2 Materials

i. Low density Polyethylene (LDPE)

ii. 2.5 L of HCl (Hydrochloric Acid) of M. W., 36.48 and purity 35.38% was supplied by BDH Chemical Ltd, Poole England ,

iii. Ethanol Absoluten $(99.7 - 100\%)$ was gotten from Johnson Solomom (Export) Ltd, London, England.

iv. NaOH(Sodium Hydroxide) of M. W. $40.0 g/mol$ was also supplied by BDH Chemical Ltd, Poole England

v. Polyvinyl Alcohol (PVA) of 98% purity was supplied by BDH Chemical Ltd, Poole England

vi. Raw kaolintic clay sample.

vii. Toluene Analar-M.W. 92.14 and $0.86 g/mol$.

viii. Alum (commercial grade),

ix. Potash (commercial grade)

x. PAnalytical XPERT-PRO Diffractometer System

xi. Phenom ProX-SEM

xii. Shimazdu FTIR-8400S

xiii. Triboscan Nanoindenta

xiv. HM8118 LCR Bridge

3.3 Preparation of Alumina From Kaolin by Acid Leaching

3.3.1 Introduction

Nanokaolin synthesis from kaolin has proved to be very challenging especially through acid leaching process owing to the various acids involved. The safe handling of the acids requires a researcher to wear protective agents and handle the acids with utmost care in order to avoid laboratory accidents. It appears to be the only option available in this case due to the ready to be used nature of the acids. The processes are Digestion, Precipitation, Peptization/Gelling/ Capping/surfactant and Drying

3.3.2 Digestion

Kaolin was first calcined for 4 hours at 600℃ in a furnace. 150g of calcined Kaolin was digested with 250 ml HCl using a KDM Style Control Mantle under reflux at the boiling point (108.6 ℃) of HCl for 70 mins. The mixture will now be precipitated.

3.3.3 Precipitation

The digested Kaolin was allowed to sediment by ageing it in the refrigerator for 18 hours. The sedimented solution was decanted and then filtered to yield a clear solution. The filterate was precipitated by the addition 25g of NaOH while keeping the temperature at about 10℃. NaOH was added to the clear solution to neutralize it leading to the formation of aluminium hydroxide precipitate in the basic medium. The gelatinous precipitate of the hydrated alumina was further

filtered under vacuum using a vacuum pump, washed repeatedly five times with distilled water and finally with absolute ethanol. The precipitate was then dried, ashed at 400℃ for one hour in a muffle furnace to burn any carbonaceous materials. The crude nanokaolin formed was stored in a desicator.

3.3.4 Peptization/Gelling

A small amount of the crude nanokaolin was weighed into a crucible and dried further for 1 hour at 400℃. 10ml of 70% nitric acid was then added to 18.100g of the hydrated alumina in a 500ml beaker. This was done with constant and vigorous stirring until it turned almost translucent. More distilled water was then added to make it up to 100ml. In a separate beaker, 5g of polyvinyl alcohol (PVA) was dissolved in 100ml of water and boiled with stirring until the colloids completely dissolves. The PVA acts as *surfactant* to control hydrolysis. After the dissolution, it was kept in the refrigerator to in order to get chilled. Both the hydrated alumina and the dissolved PVA were mixed together and stirred for 40 minutes. This process of adding PVA to alumina and mixing is called *capping*.

After the capping, ammonia was added to make the PH to 8. At this point the solution turns into a thick gel due to condensation. Again the mixture was finally stirred for 40 minutes to age the sample and poured on a filter paper and allowed to dry at 60℃ in a hot oven

3.3.5 Drying

The dried sample is broken to pieces and calcined in a furnace at 600 ℃ for 4 hours to burn out the remaining carbonaceous materials such as PVA and volatile ammonium nitrate contaminants. The process also helps to crystallize the alumina (Nanokaolin).

3.3.6 Doping

Alumina was first dispersed in toluene and stirred to dissolve for 15 mins before compounding process. The dissolved alumina was then compounded with LDPE matrix using a magnetic mixer at 60 rpm for 12min at different weight ratios. The samples were finally achieved by mixing certain percentage of alumina with LDPE.

3.4 Preparation of LDPE/Alumina Nanocomposites

Below is the schematic representation of described preparation process leading to the samples.

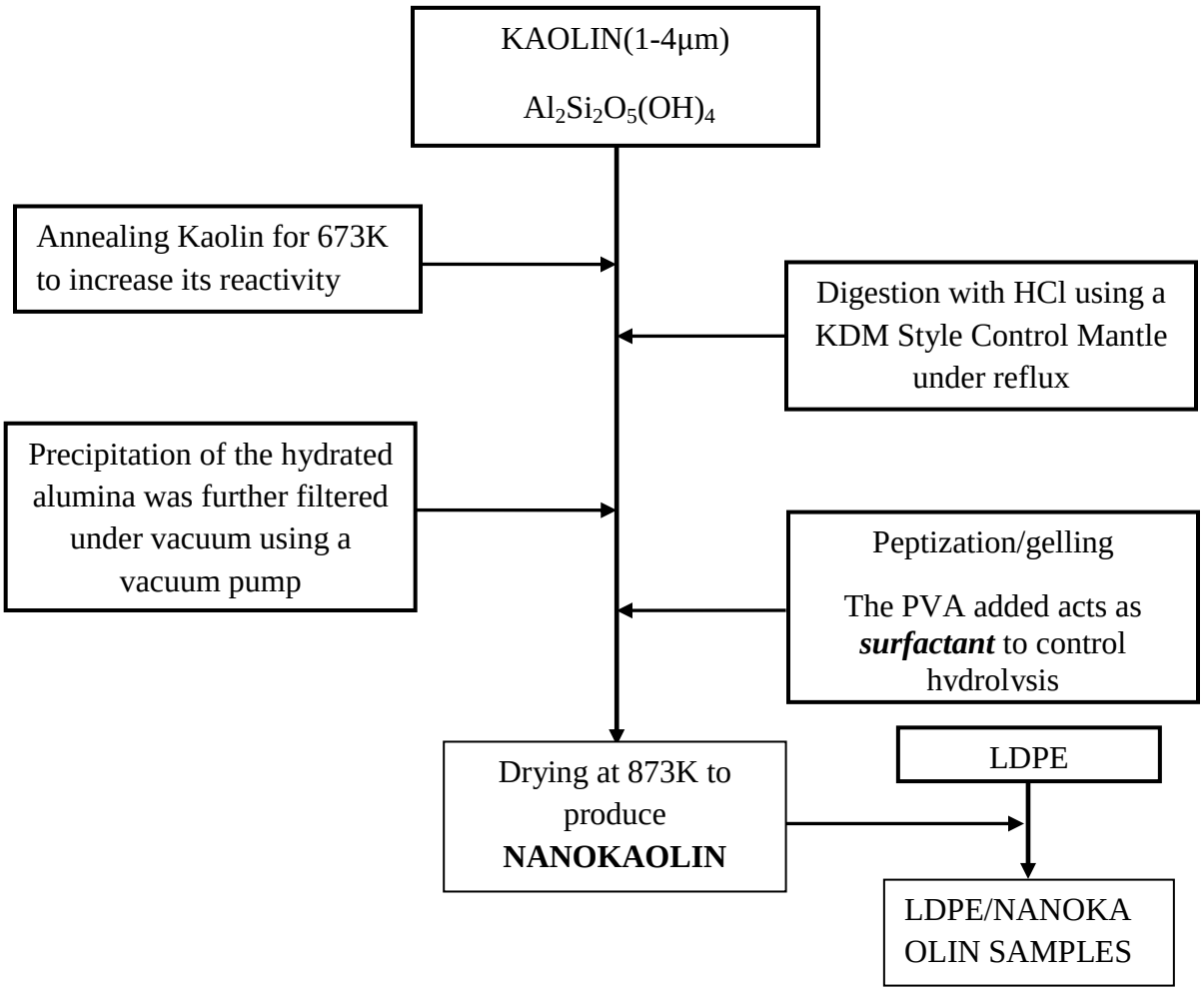

Fig 3.1: Schematic diagram of preparation of sample

TABLE 3.1: Composition of LDPE with various percentage weight of alumina.

Sample	Alumina Percentage (%)wt
PEK 1	0
PEK 2	0.5
PEK 3	1.0
PEK 4	1.5
PEK 5	2.0
PEK 6	2.5
PEK 7	3.0
PEK 8	3.5
PEK 9	4.0
PEK 10	4.5
PEK 11	5.0

3.5 Preparation of Nanocrystalline Alumina from Alum via Thermal Sintering

Potash (671.7 g) was dissolved in boiling water and allowed to sediment for 24hours. The potash was decanted after 24hours. 326g of alum was allowed to dissolve in hot water. After dissolution of alum, it was neutralized with the sedimented potash. Since the mixture needs to be made basic, addition of potash stops as soon as it stops bubbling and when the PH is about 7.5 or 8. The mixture was confirmed with a red litmus paper to turn blue. It was chilled to 25℃ and added to potash and filtered. The mixture was washed several times with distilled water (5 litres was use). The precipitate was now dissolved in concentrated Nitric acid and dried under heat. This

was then further fired in a furnace at a temperature of 1000℃ for 2 hours leading to the formation of flake-like alumina.

3.6 Characterization of Nanocomposites

The nanocomposites of layered clay/LDPE were characterized by performing characterization techniques described below. The effects of the layered clay addition on the microstructural, electrical and mechanical properties of the nanocomposites were investigated in comparison with the properties of ordinary LDPE.

3.6.1 Structural investigation

3.6.1.1 X-ray diffraction (XRD)/ PANalytical XPERT-PRO Diffractometer System

To investigate the effect of alumina on the intercalation of the LPDE layers XRD technique was employed. The modification of the LPDE is not intended to structurally change its flexibility and mode but rather to examine whether the samples so formed are exfoliated, intermediate or intercalated nanocomposites. XRD was carried out using a PANalytical XPERT-PRO diffractometer system with a Reflection-Transmission Spinner configuration on a PW3064/60 sample stage for powder diffraction. A Gonio scan axis with a start position of 5.0464 (2Θ) and end position of 99.9184 was employed using a step size (2Θ) and scan time (s) of 0.067 and 29.8450 respectively. The scan mode was continuous with a specimen length of 10mm ray-length and measurement was conducted at room temperature of 25˚C. The generator setting employed was 30 mA and 40 kV with K-Alpha 1 (Å) wavelength of 1.54060 using Copper (Cu) as the anode material. In cases where the scan time and setting differs, it will be stated.

3.6.1.2 Scanning Electron Microscopy (SEM)/ Phenom ProX SEM

Dispersion of the silicate layers in the polymer matrix was investigated by using SEM (Scanning electron microscopy (Phenom ProX) from the fractured surface of the tensile samples. The magnetic mixer rotor speed used was set at 60rpm which was the standard observed from other works Mehdi et al,(2015).1 The primary goal of using SEM was to determine particle size for interphase analysis, and to determine particle dispersion (Ciprari, 2004). It also reveals local topography in the early stage of the growths of a crystal.

Some unspecified quantity of sample was placed on a double adhesive sticker placed in a sputter coater machine for 5sec before placing the sample in the SEM to give the sample a conductive property, and this will not affect the quality of the images. Sample stub was fixed on a charge reduction sample holder, then was changed into the machine column thereafter the doors of the SEM was closed

Machine was allowed to stabilize for some seconds, the parameters to be used were then set. 15kV was used in imaging the sample set at 1000x magnification and was focused using a rotary knob until a clear and proper image was produced in a NavCam mode, this was then transferred to an electron imaging mode. The image was then transferred to Phenom suite software where fibermetric/pore measurements were carried out after contrasting/ brighten, after the spots where all analyzed then a report was generated by the machine and was saved in a folder using the name of the sample used. Same was used in determining the pore measurement and fiber present in the sample.

A: MODEL -PHENOM ProX Scanning Element Microscope

B: Sample holder

Plate: 3.1 (A) MODEL -PHENOM ProX Scanning Element Microscope, (B) Sample holder

3.6.1.3 Fourier Transform Infrared Spectroscopy (FTIR)/ Shimazdu FTIR- 8400S

Shimazdu FTIR- 8400S Fourier Transform Infrared Spectroscopy was used in National Research Institute for Chemical Technology (NARICT), Zaria to identify the functional groups and finger prints of the samples obtained from the spectra produced. The sample holders were cleaned with methanol and then with acetone thoroughly and the thin films of the samples were placed on the spectrometer measurement cell. The samples were then scanned with infrared radiation through frequency range expressed as wave number of 4000 cm^{-1} to 400 cm^{-1} to obtain the spectrum for each sample. Finally the amount of radiation absorbed by the sample whose reciprocal is transmittance was plotted against the wave number of the absorbed radiation.

3.7 Measurement of Mechanical Properties

3.7.1 Nanoindentation/ Triboscan nanoindenta

Triboscan nanoindenta was used to determine elastic modulus and hardness properties. Samples for nanoindentation was made to be flat and may be microns thin and millimeters wide or long. Thin film samples on glass slides were created to support nanoindentation. The samples were prepared by compression molding, annealing at 110–200 ℃, and cooling to room temperature. The resulting samples are with a flat surface on the thin film. All samples were prepared using similar procedures, although slight variations were used in an attempt to minimize air bubbles in the samples.

3.8 Measurement of Electrical Properties

HM8118 LRC Bridge with frequency response in the range of 20 to 200 kHz was used to measure the capacitance, and the dissipation factor was read directly from the bridge. The electrical parameters (impendence z, dielectric permittivity ε', dielectric loss ε'' and ac conductivity σ_{ac}) were calculated from conductance G_s and capacitance C_s which were measured using the LCR meter.

Plate 3.2 : HM8118 LRC Bridge with the designed sample holder

3.8.1 Impedance change within the frequency range of 20 khz-180 khz

The dielectric properties of the solid samples were studied using a two-electrode coaxial dielectric test cell designed specifically for the research. HM8118 LRC Bridge with frequency response in the range of 20 to 200 kHz was then used to measure the capacitance, and the

dissipation factor was read directly from the bridge. The LCR was used to take the impedance variation along the said frequency range in order to examine the fall of the impedance as the frequency is increased.

3.8.2 Dielectric constant and loss factor

The dielectric constant measurement, also known as relative permittivity, is one of the most popular methods of evaluating insulators such as rubber, plastics, and powders. It is used to determine the ability of an insulator to store electrical energy. The complex dielectric constant consists of a real part (ε), which represents the storage capability and an imaginary part (D), which represents the loss.

Dielectric constant measurements can be performed easier and faster than chemical or physical analysis techniques making them an excellent material analysis tool. The dielectric constant is defined as the ratio of the capacitance of the material to the capacitance of air, or

$$\varepsilon = \frac{C_x}{C_0} \qquad 3.1$$

where Cx = capacitance with a dielectric material and Co = capacitance without material, or vacuum. The ε value of dry air is 1.00053, which for most measurement applications is usually close enough to the value of a vacuum, which is 1.0000. Thus if a material is to be used for insulating purposes only, it would be better to have a lower dielectric constant, or as close to air as possible. To the contrary, if a material is to be used in electrical applications for storage of electrical charge, the higher the dielectric constant the better. More charge is stored when a dielectric is present than if no dielectric (air) is present. The dielectric material increases the

storage capacity of the plate capacitor, hence the dielectric constant of any solid or liquid would be greater than 1(Tong, 2010).

3.8.3 Complex electric modulus

Dielectric constant of materials often varies with applied frequency, primarily because the polarization is strongly affected by the frequency. This frequency dependence implies that material does not respond instantaneously to an applied field upon polarization. Therefore, the response of materials to an alternating field is characterized by complex electric modulus defined as:

$$M^* = \frac{1}{\varepsilon^*} = \frac{1}{\varepsilon' - i\varepsilon''} = \frac{\varepsilon' + i\varepsilon''}{(\varepsilon' - i\varepsilon'')(\varepsilon' + i\varepsilon'')} = \frac{\varepsilon'}{(\varepsilon'^2 + \varepsilon''^2)} + i\frac{\varepsilon''}{(\varepsilon'^2 + \varepsilon''^2)} = M' + iM'' \qquad 3.7$$

where the calculated values of dielectric permittivityε', and dielectric loss factor ε'' were used to calculate the real part(M'), and imaginary part (M'') of electric modulus.

CHAPTER FOUR

4 RESULTS AND DICUSSIONS

4.1 Introduction

This chapter presents the results and interpretations of influence of the nanoparticles (alumina) on the structural, mechanical, electrical and chemical properties of polyethylene composites. In this study, Scanning Electron Microscope(SEM), X-Ray Diffraction(XRD) andFourier Transform Infrared(FTIR) for the morphological analysis; nanoindentation for mechanical testing techniques, LCR for the electrical measurement and XRF for the evaluation of the chemical composition before and after doping. Before doping the low density polyethylene with the nanophase kaolin that gives the various samples at varying composition, the nanosize of the kaolin will have to be confirmed first by XRD using the Sherrrer's formular.

4.2 Experimental Results

4.2.1 Structural study

4.2.1.1 X-RAY DIFFRACTION (XRD)

This section describes the XRD results and interpretation as obtained from PANalytical XPERT-PRO diffractometer system with a view of deriving the structural phases from samples prepared. Before doping the low density polyethylene with the alumina that gives the various samples at varying composition, the nanosize of the alumina was confirmed by the use of the well-known Scherrer formula the average crystallite size, L, is:

$$L = \frac{K\lambda}{\beta . COS\theta} \qquad 4.1$$

Where λ is the X-ray wavelength in nanometer (nm), β is the peak width of the diffraction peak profile at half maximum height resulting from small crystallite size in radians and K is a constant

related to crystallite shape, normally taken as 0.9. The value of β in 2θ axis of diffraction profile must be in radians (Cullity and Stock, 2001).

The XRD result is expected to give the lattice parameters like phase identity, phase purity crystallinity, crystal structure and percent phase composition as following information required from the samples.

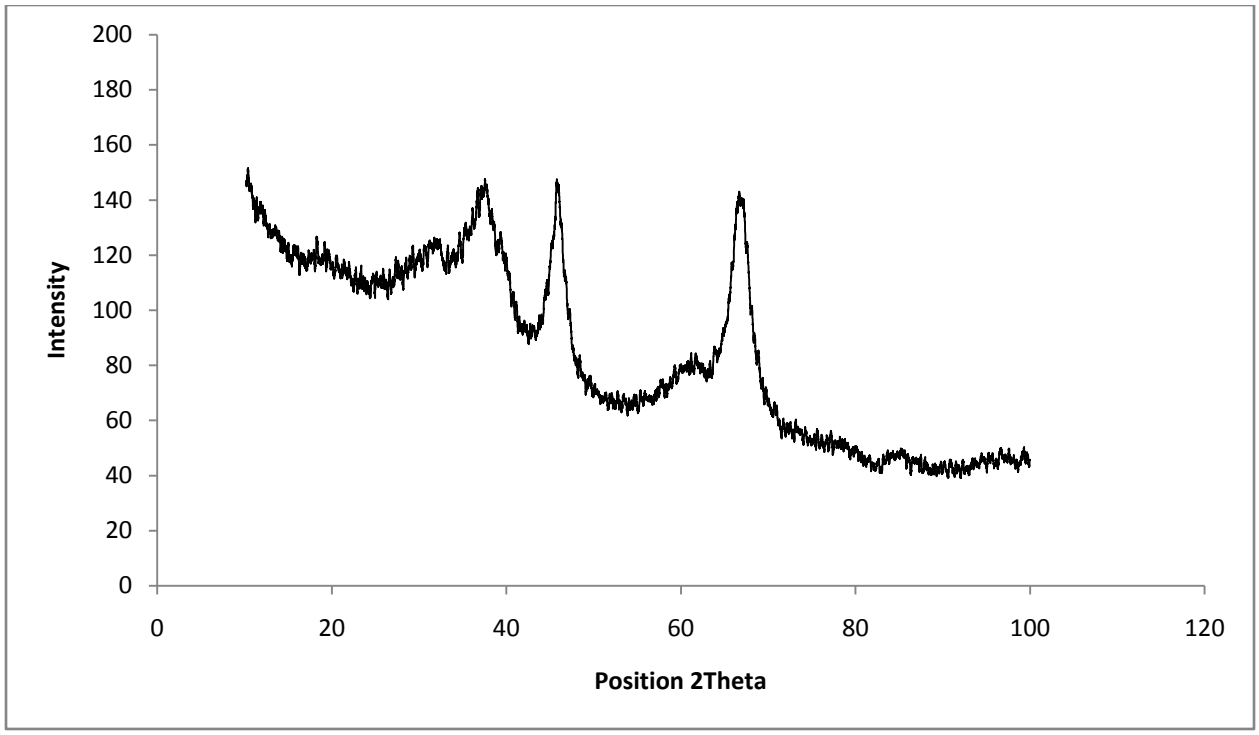

Fig 4.1: XRD of pure Nanokaolin(alumina) from Kaolin

In this work, the [2θ] peaks are visible at 36, 46 and 66 respectively. From fig 4.1, the pure alumina sample was matched with a reference code of 01 – 075 – 0921, compound formula and name of γ- (Al_2O_3)1.33 and aluminum oxide. The sample had a cubic crystal system, Fm-3m space group . The [*hkl*] value was calculated to be [*200*] from ICDD using POWD-12++ (1997).

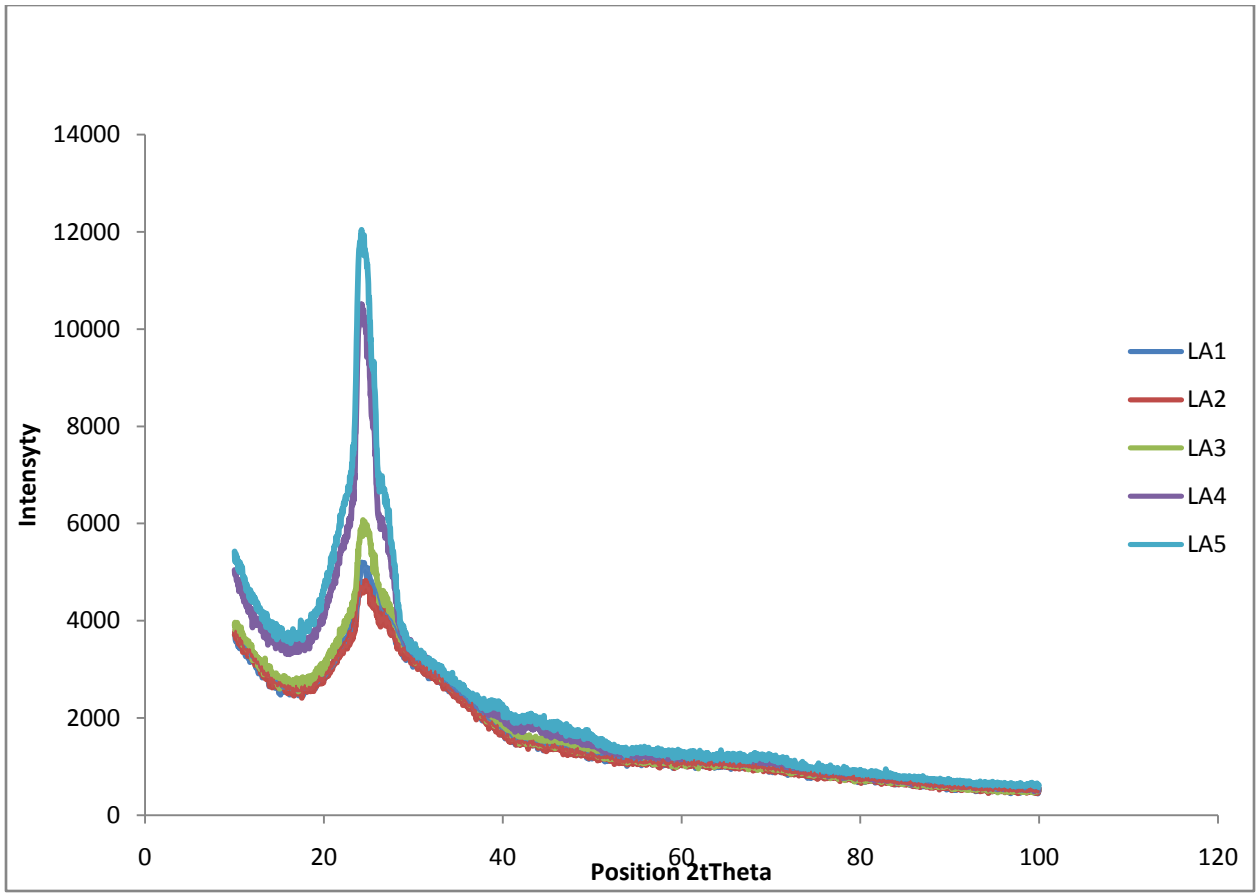

Fig 4.2: X-ray diffraction patterns of LDPE/alumina nanocomposites

Fig 4.2 shows the XRD results of LDPE doped with alumina at 1%wt, 2%wt, 3%wt 4%wt and 5%wt tagged as LA1,LA2 LA3, LA4 and LA5 respectively. During the experiment, the intensity diffracted by a semicrystalline polymer was measured as a function of Bragg angle 2[θ].

LA1 and LA2 appeared to overlap at the same intensity. As more alumina was added, an increase in the intensities of the peak was observed. This is a characteristic behaviour of polymers as reported in earlier works (Song *et a.l*, 2007 and Supri *et al.*, 2008). The XRD patterns of all the images show peaks at about 21.9012, 23.8958, and 25.7284[2Θ], at various intensities.

4.2.1.2 Scanning Electron Microscope (SEM)

The SEM techniques studies the structural changes that occur on the surface by giving an insight into the structural arrangements in this case of polymer surface, absorbents and interfacial solvent molecules in the electrical double layer. It also allows the study of the charge transfer reactions and absorption processes occurring at the surface of electrified double layer to be altered. Each of the samples reported was subjected to the same procedures to get the desired structure. The structures obtained using SEM measurements are as follows:

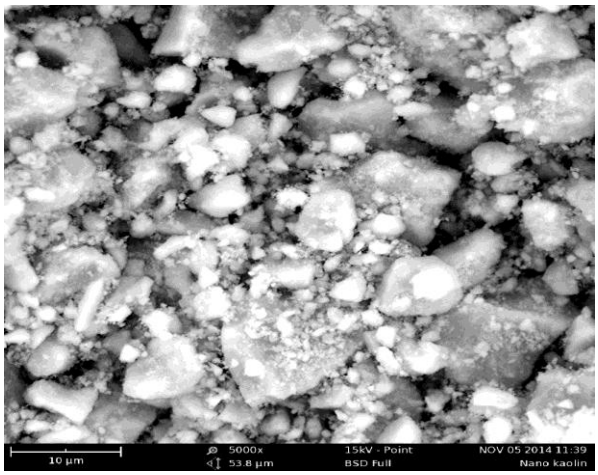

Plate 4.1. Backscattered SEM image of alumina from kaolin synthesised by acid leaching, filtration and drying taken at 15kV demonstrating foamy agglomerates at low magnifications (5000x) and presence of well-built voids in their

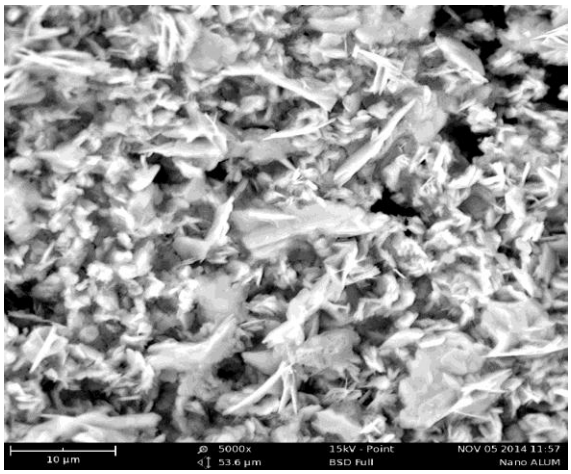

Plate 4.2. Backscattered SEM image of alumina from alum synthesised by combustion technique structure showing flakes forms of the alumina

Fig 4.3 is the SEM morphology of the solid phase of alumina from kaolin after acid leaching, filtration and drying. It shows the formation of foamy agglomerates at low magnification (5000x) and the presence of larger voids in theirs structures at high magnification (20000x) especially plate 4.1 and plate 4.2. Fig 4.4 shows that the powders have flake like form of morphology, which makes them brittle and easy to crumble powders.

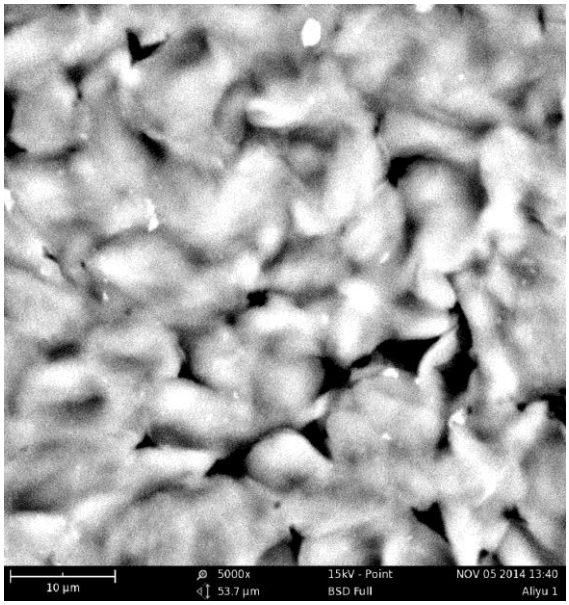

Plate 4.3. Backscattered SEM image of LDPE doped with 0.5% w/w Alumina.

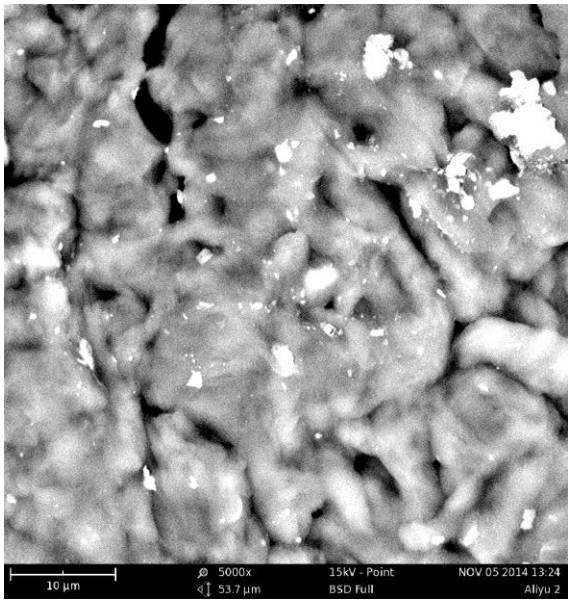

Plate 4.4. Backscattered SEM image of LDPE doped with1% w/w Alumina

In plate 4.3 and plate 4.4, the dispersion of the alumina was non-uniform even though it was expected to be uniformly dispersed into the LDPE matrix. But however, there appears to be a little bit of agglomeration of the nanoparticles which must have hindered uniform dispersion into the matrix.

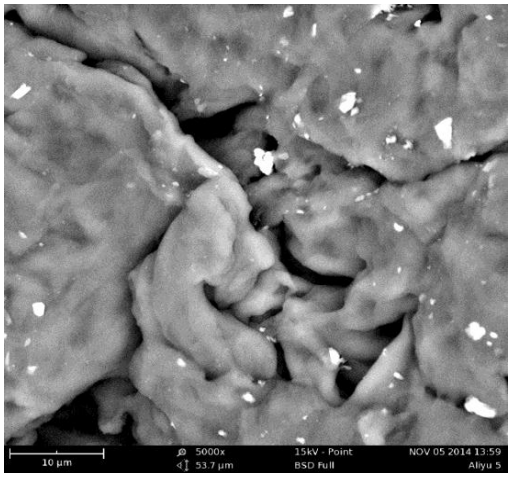

Plate 4.5. Backscattered SEM image of LDPE doped with 1.5wt Alumina

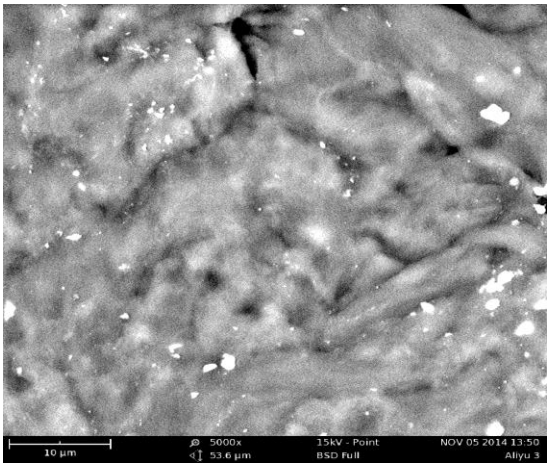

Plate 4.6. Backscattered SEM image of LDPE doped with 2.0wt Alumina

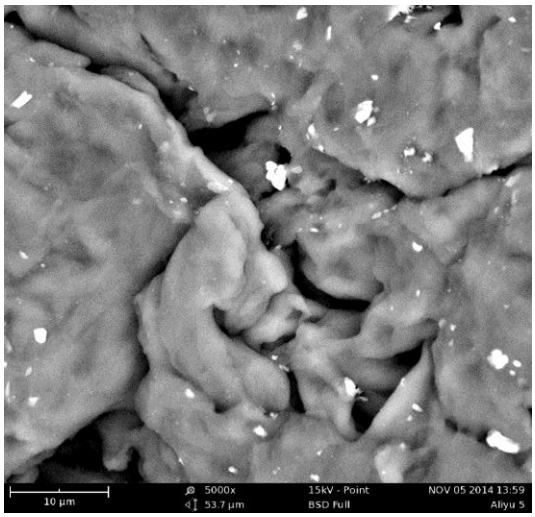

Plate 4.7 : Backscattered SEM image of LDPE doped with 2.5wt Alumina

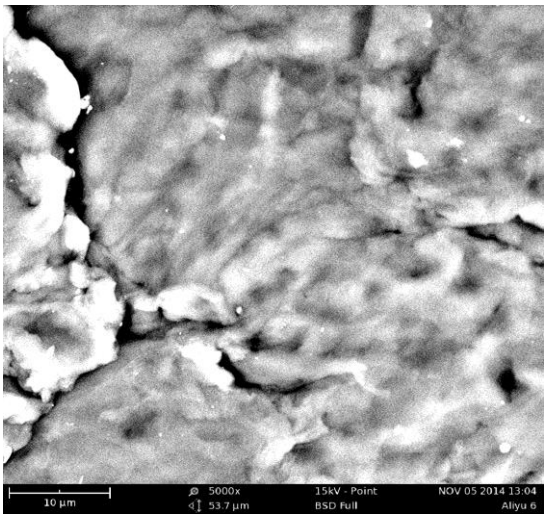

Plate 4.8: Backscattered SEM image of LDPE doped with 3.0wt Alumina

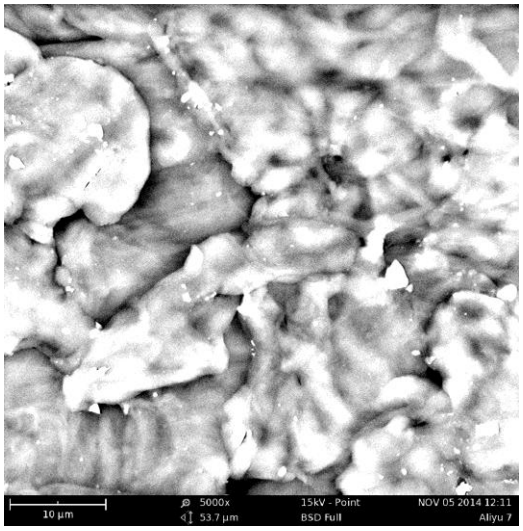

Plate 4.9. Backscattered SEM image of LDPE doped with 3.5wt Alumina

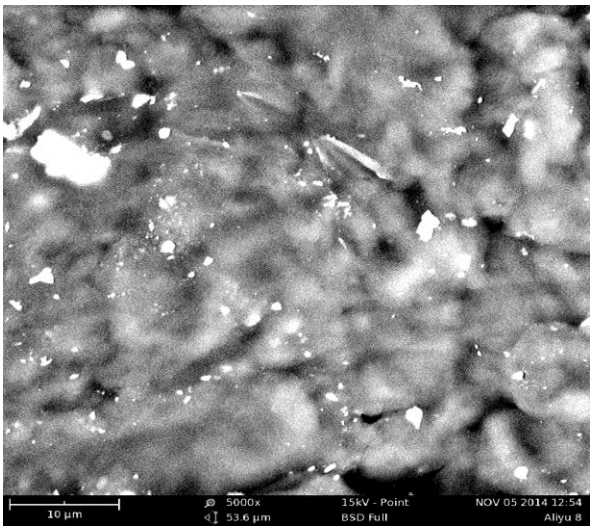

Plate 4.10. Backscattered SEM image of LDPE doped with 4.0wt Alumina

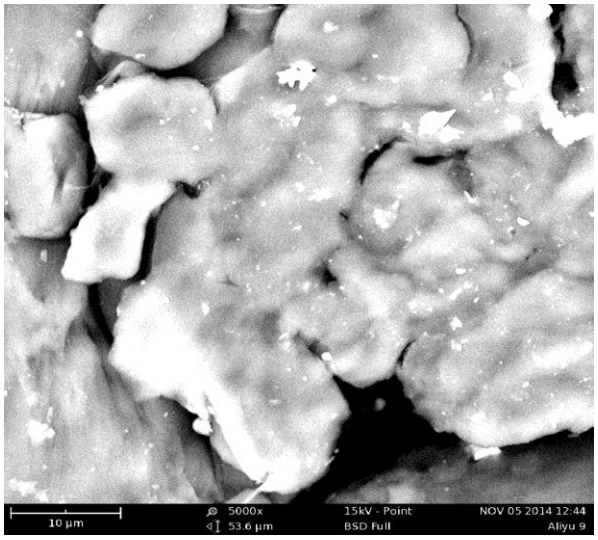

Plate 4.11: Backscattered SEM image of LDPE doped with 4.5wt Alumina

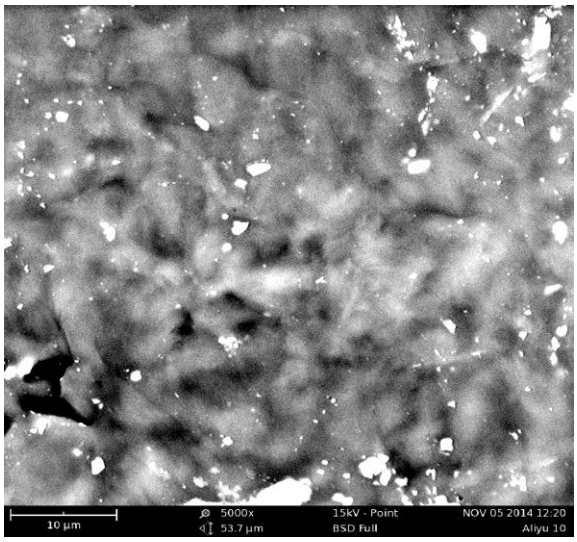

Plate 4.12: Backscattered SEM image of LDPE doped with 5.0wt Alumina

In Plate 4.5- 4.10, addition of alumina becomes more pronounced and more scattered across the matrix. SEM images also revealed a heterogenous dispersion of nanoparticle layers in the LDPE matrix. On closer inspection of the alumina in the figures, flocculation appears to have occurred since the larger mass appears to be an assortment of the smaller particles retaining their individual structure. According to (Ciprari, 2004), it is not clear whether the particles flocculated before or after interaction with the polymer, since the polymer layer on each smaller particle could be disguised by additional polymer coating or by the sputter coating.

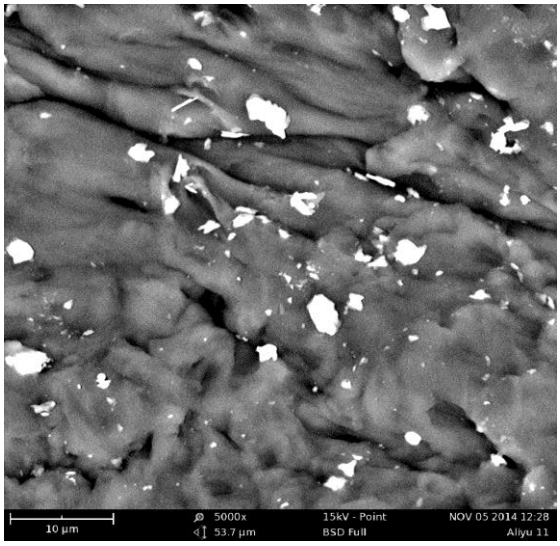

Plate 4.13: Backscattered SEM image of LDPE doped with 5.5wt Alumina

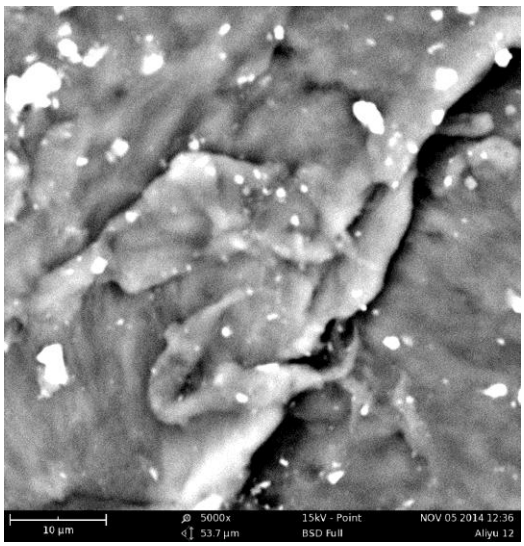

Plate 4.14. Backscattered SEM image of LDPE doped with 6.0wt Alumina

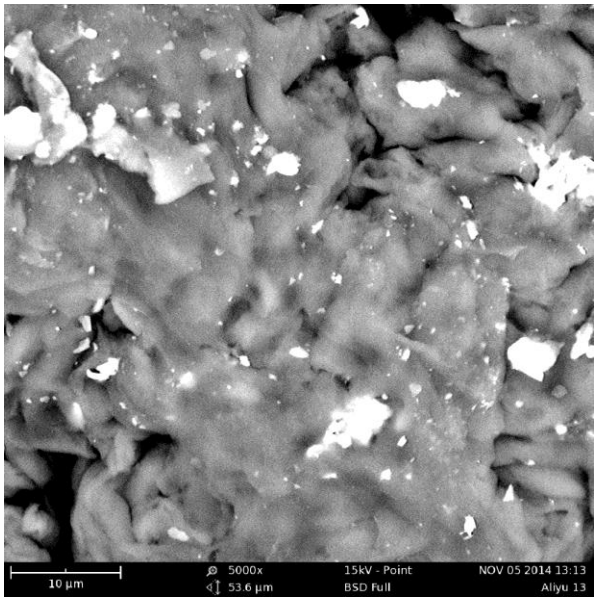

Plate 4.15. Backscattered SEM image of LDPE doped with 6.5wt Alumina.

The images of Plate 4.3-4.15, appears to show an indication that an intermediate nanocomposites has been produced ie partially intercalated and partially exfoliated. This is important to note because agglomerated products are usually made to a specification that requires some knowledge

of its use/functionality of the material required. It is unknown whether the particles flocculated immediately after being mixed and capped in the NaOH, or if flocculation occurred sometimes during the simple heating periods as the last step of preparation with the aim of making the samples more compacted.

4.2.1.3 Results of fourier transform infrared spectroscopy (FTIR)

Infrared spectroscopy is a technique based on the vibrations of the atoms of a molecule. An infrared spectrum is commonly obtained by passing infrared radiation through a sample and determining what fraction of the incident radiation is absorbed at a particular energy. The energy at which any peak in an absorption spectrum appears corresponds to the frequency of a vibration of a part of a sample molecule. (Barbara, 2004)

In this case, Infrared (IR) spectroscopy [invariably Fourier transform infrared spectroscopy (FTIR)] is used to determine a variety of molecular characteristics of polyethylene. It may be used to identify and quantify various additives and chemical groups attached to the polyethylene backbone. Additionally it can provide information with respect to solid-state morphology. (Andrews, 2000). FTIR) finds two principal applications in the morphological analysis of polyethylene, these being the determination of orientation and of local degrees of ordering within the sample. The latter involves the determination of the fractions of the sample that are crystalline (ordered), liquidlike (disordered), and interfacial (partially ordered).

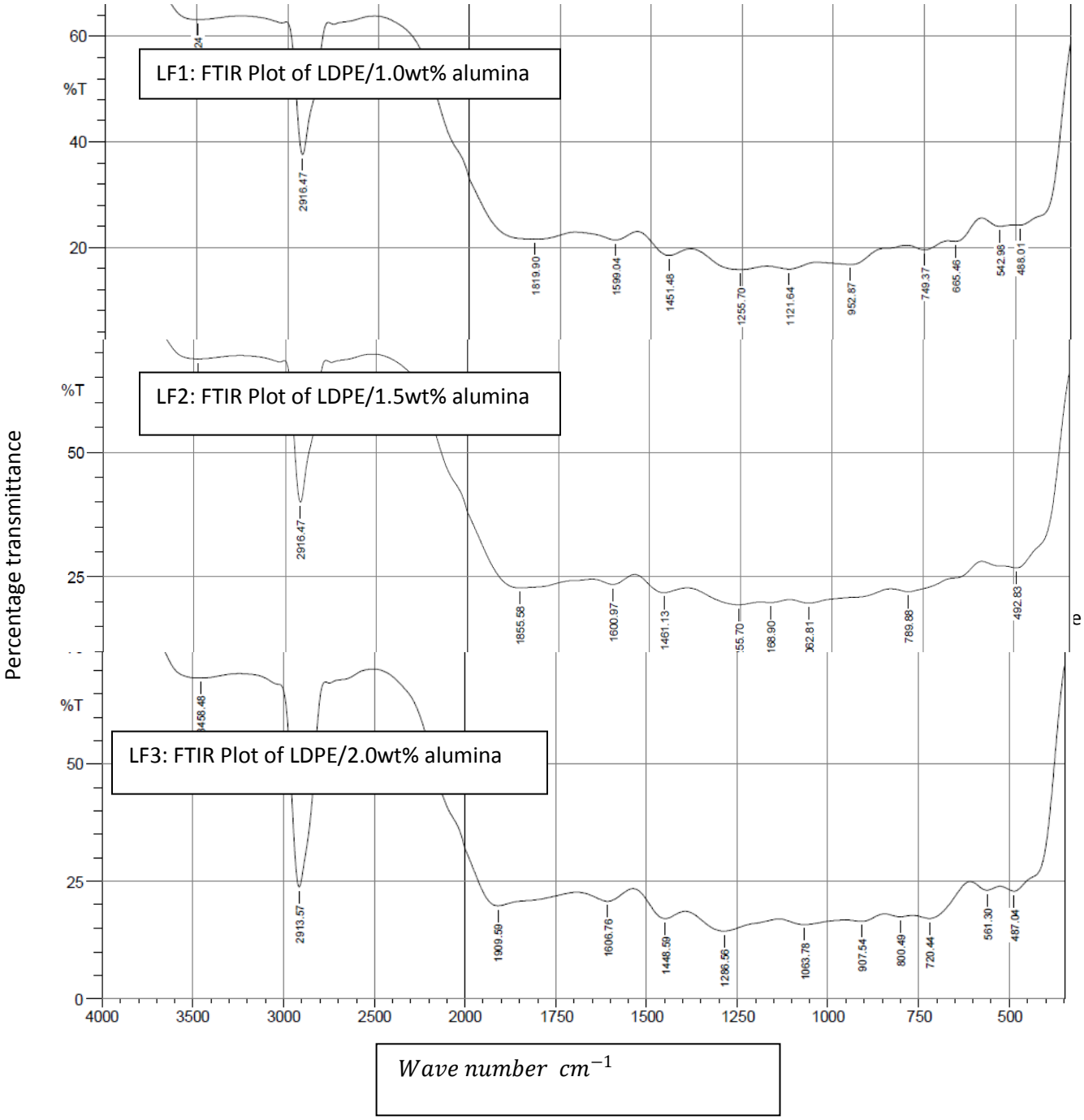

Fig 4.3: Plot of transmittance versus wave number LF1, LF2 & LF3

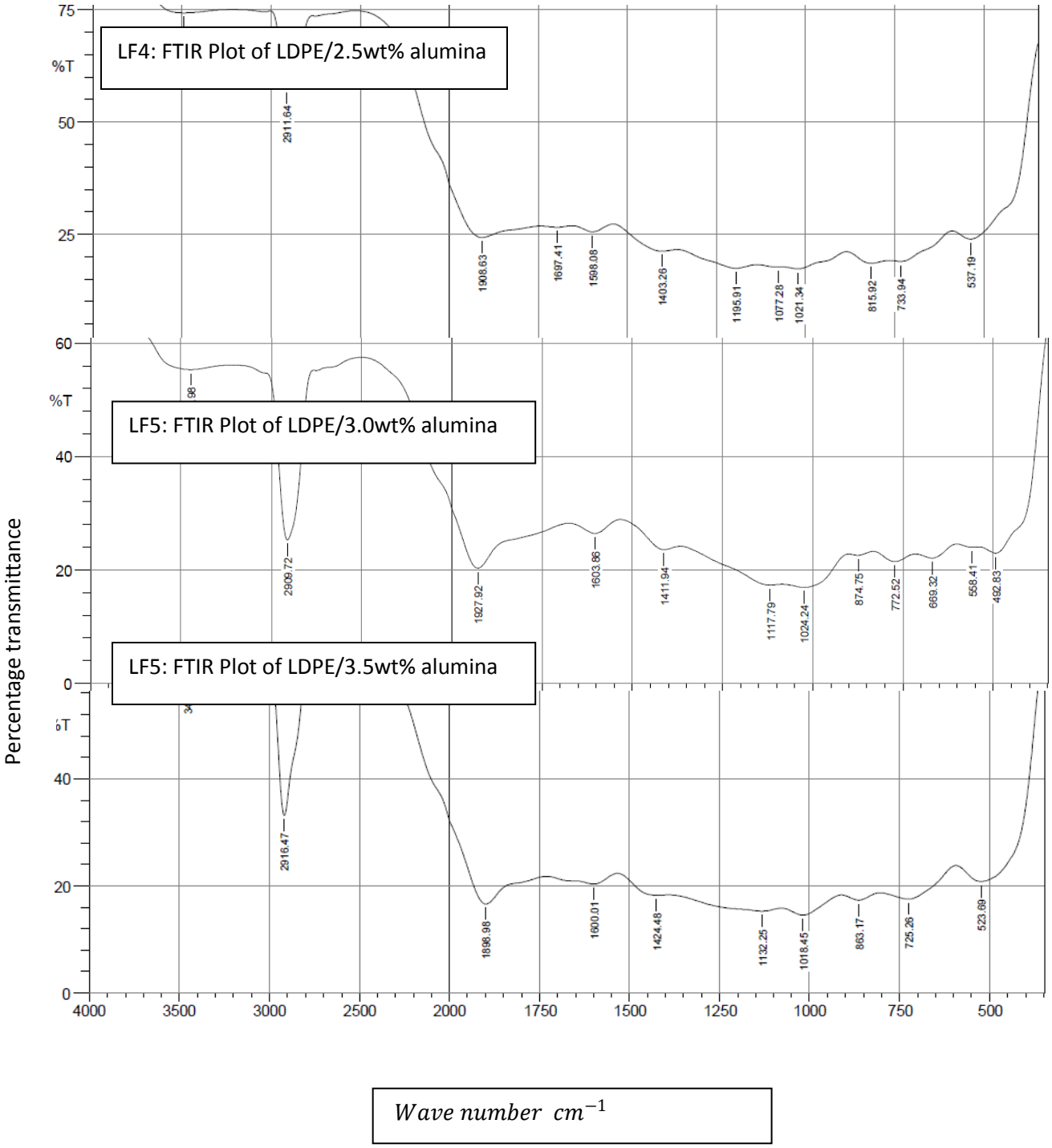

Fig 4.4: Plot of transmittance versus wave number for LF4, LF5 & LF6

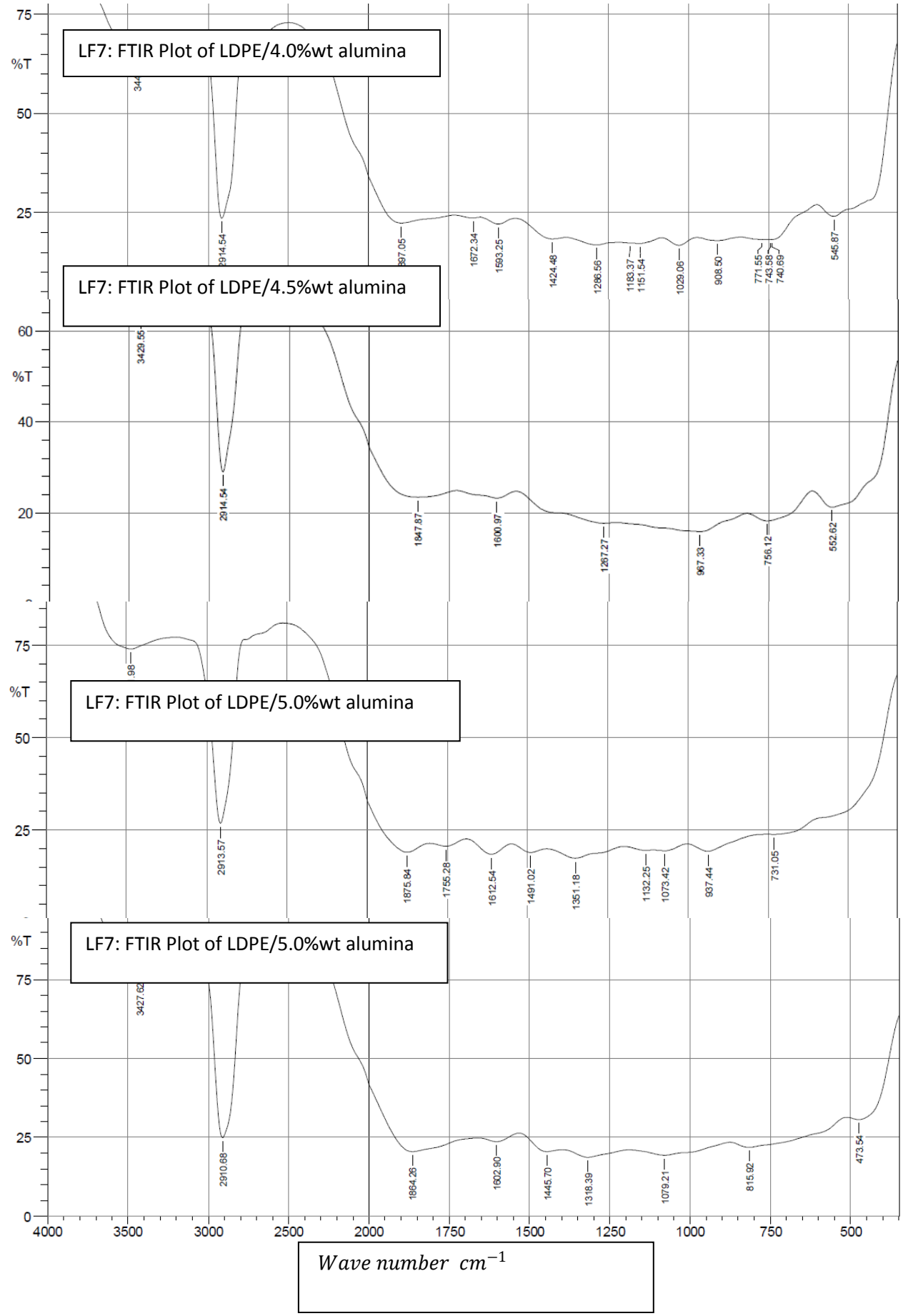
LF7: FTIR Plot of LDPE/4.0%wt alumina
LF7: FTIR Plot of LDPE/4.5%wt alumina
LF7: FTIR Plot of LDPE/5.0%wt alumina
LF7: FTIR Plot of LDPE/5.0%wt alumina
%T
Percentage transmittance
Wave number cm^{-1}
4000
3500
3000
2500
2000
1750
1500
1250
1000
750
500

Fig 4.5: Plot of transmittance versus wave number LF7, LF8 LF9 & LF10

Table 4.1: The FTIR Table showing relative intensity and functional groups

Frequency cm^{-1}	Relative intensity											
	PA1	PA2	PA3	PA4	PA5	PA6	PA7	PA8	PA9	PA10	Functional group	Bond
3500-3200	s	s	s	s	s	s	s	s	s	s		O-H stretch
3000-2850	m	m	m	m	m	m	m	m	m	m	Alkanes	C-H stretch
1740												
1650-1580	m	m	m	m	m	m	m	m	m	m	1° amine	N-H Bend
1500-1400	m	m	m	m	m	m	m	m	m	m	aromatic	C-C Stretch (in-ring)
1335-1250	s	s	s	s	s	s	s	s	s	s	aromatic amine	C-N stretch
-1320-1000	s	s	s	s	s	s	s	s	s	s	Alcohol, esters, ethers carboxylic	C-O stretch
900-675	s	s	s	s	s	s	s	s	s	s	aromatics	C-H, "oop"
850-550	m	m	m	m	m	m	m	m	m	m	Alkyl halides	C-Cl stretch

Key: s=strong, w=weak and m=moderate/medium

Fig 4.3 (LA1), is the FTIR a pure LDPE. It has about 12 peaks with $3492.24cm^{-1}$ as the maximum value which is typical of O-H stretching. The IR absorption spectra for doped LDPE with different alumina concentration are shown in fig (4.3 - 4.5). The spectra show as absorption peaks at this range $(3500\text{-}3200)cm^{-1}$refers to the intermolecular hydrogen bonding and $-OH$

stretch vibrations. The vibrational band observed at $2916.47\ cm^{-1}$ which appears in all the doped samples with little variation, is associated with the $C-H$ stretching from alkyl groups.

In $N-H$ bending, the vibrations occur at frequency lower than $C=H$ absorption band. In mulls and pellets, the band occurs near 1655-1620cm^{-1} and is usually under the envelop of the amide I band. In dilute solution, the band appears at lower frequency 1620-1590cm^{-1} and normally is separated from amide I band (Robert et al, 2005).

In $C-N$ stretching vibrations, medium to weak absorption for the unconjugated $C-N$ linkage in primary, secondary, and tertiary aliphatic amines appears in the region $1250-1020cm^{-1}$. The vibrations responsible for this bands involve $C-N$ stretching coupled with the stretching of adjacent bonds in the molecules. Aromatic amines display strong $C-N$ stretching absorption in the region $1342-1266cm^{-1}$. The $C-O$stretching vibration in alcohols and phenols produce a strong band in the $1260-1000cm^{-1}$ region of the spectrum. The $C-O$stretching mode is coupled with the adjacent $C-C$ stretching vibration; thus in primary alcohols the vibration might better be described as asymmetric $C-C-O$ stretching vibrations (Barbara, 2004).

Robert *et al*.,(2005) claimed that the in-phase and out-of-plane bending of a ring hydrogen atom is strongly coupled to adjacent hydrogen atoms. The position of absorption of the out-of-plane bending bands is a characteristic of the number of adjacent hydrogen atoms on the ring. These band are intense and frequently appear in the region 900 – 675 cm^{-1}.

These main LDPE characteristic peaks are observed in all doped samples; which indicates that the alumina molecules are interstitially distributed across the LDPE matrix without forming any chemical bonding between them at the specified condition of the research.

The main difference observed in all the figures thereafter due to the addition of alumina is either there is shift in the position of some peaks or the appearance new peaks as more alumina is added, and also the stretching mode of certain peaks or both.

4.2.2 Mechanical characterisation

4.2.2.1 Nanoindentation

Nanoindentation was performed on all the samples to determine the localized mechanical properties of polymer nanocomposites. Thin film samples were prepared and tested for all systems. The parameters used for each test series were the same except for the different contact depth and contact area. Nanoindentation software performed all calculations of young's modulus and hardness based on the input parameters, and generated 3D topography plotting between maximum force exerted on the sample to the indentation depth for each sample.

When a polyethylene sample is subjected to external stress there is an initial deformation prior to yield that is homogeneous and is largely recoverable when the stress is removed. This initial region of elasticity can vary from 1% to 2% for highly crystalline samples up to 50% or more in high co-unit copolymers and ionomers (Andrew, 2000).

From Fig 4.21, and Fig 4.22, there was increase in hardness and elastic modulus across all the doping points. The hardness of ordinary LDPE is $13.5MPa$ Andrews (2000). After doping with alumina, it was found to have increased within the range of $(14-34MPa)$ in this work. As for elastic modulus, (Maziyar *et al.*, 2014) got a maximum of $0.48GPa$ by using carbon nanotubes on LDPE while this work produced $(0.74-1.44GPa)$. This may be associated with the fact that the alumina used in this work is denser than the carbon nanotubes used by Maziyar and Hassan (2014).

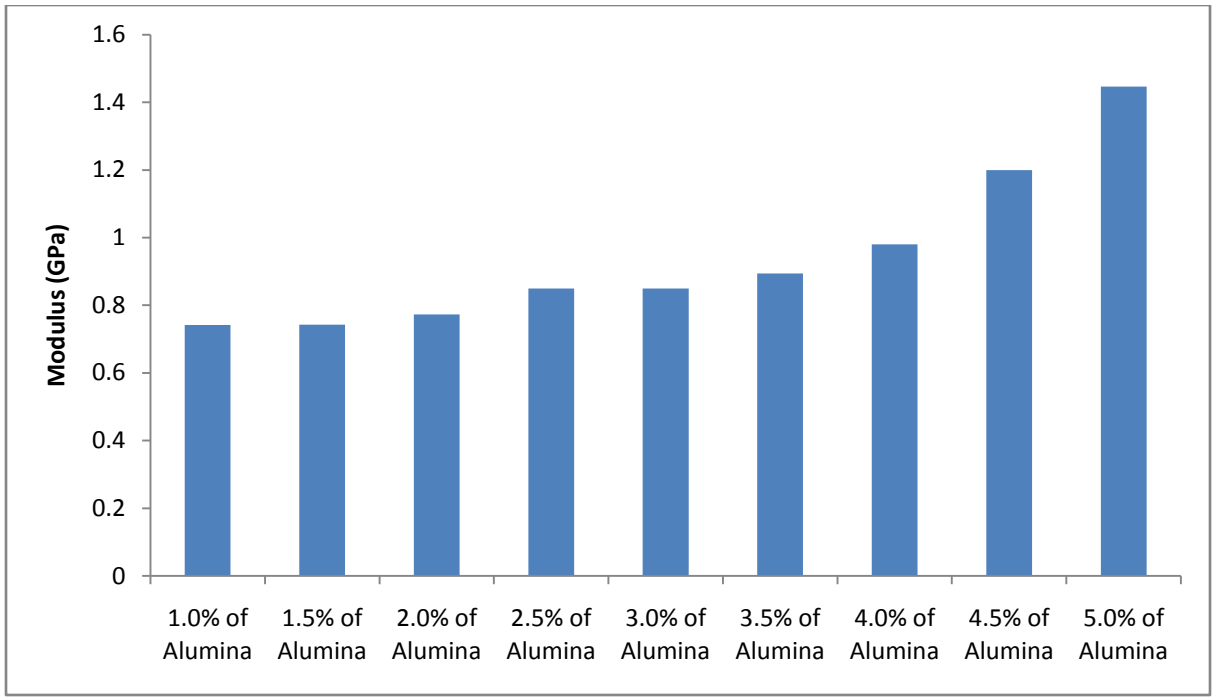

Fig 4.6: Nanoindentation elastic modulus summary results showing the variation of modulus with concentration of alumina

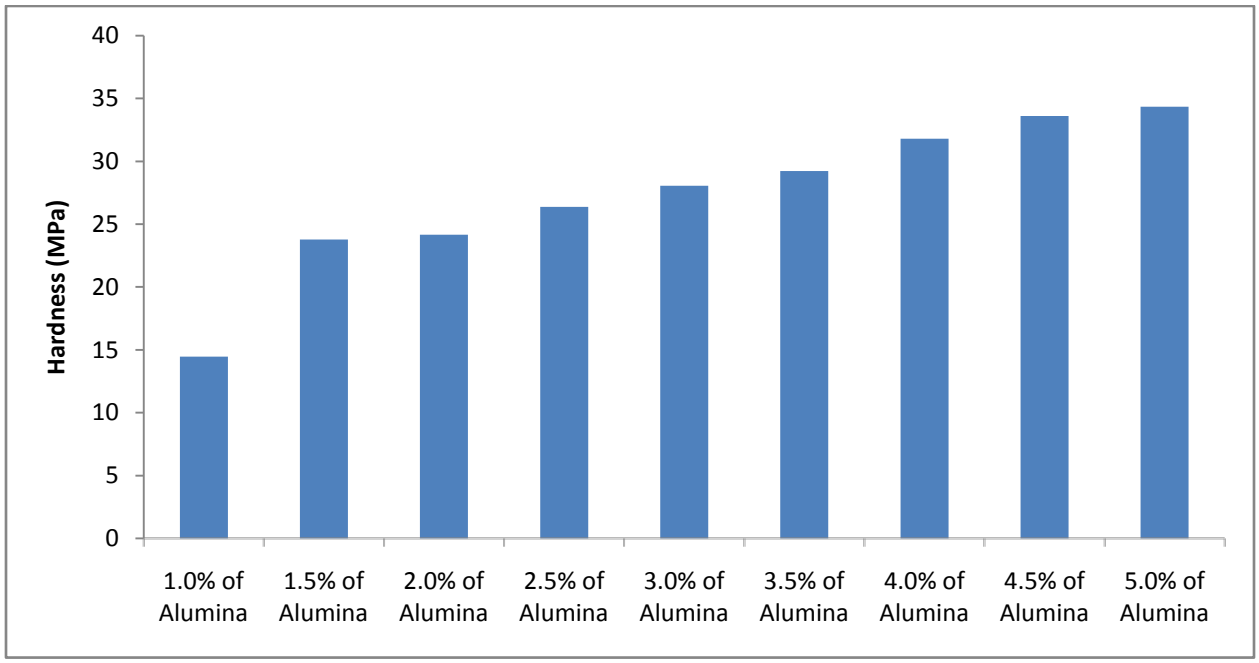

Fig 4.7: Nanoindentation hardness summary results showing the variation of hardness with concentration of alumina.

4.2.3 Electrical measurement

The electrical measurement of LDPE/alumina samples seeks to determine the response of the samples to various types of electric fields. This was done by measuring the capacitances at varying frequencies and the relative permittivities and conductivities were determined in order to get the optimum value for the dielectric constant.

4.2.3.1 Dielectric permittivity response with frequency

The dielectric measurements were carried out in the frequency range of 20 – 200 kHz. Fig 4.4.1 shows the variation of dielectric permittivity at different frequencies for doped LDPE at different percentage weights. The plots clearly show that dielectric permittivity for all the samples remained slightly constant up to about 100 kHz.

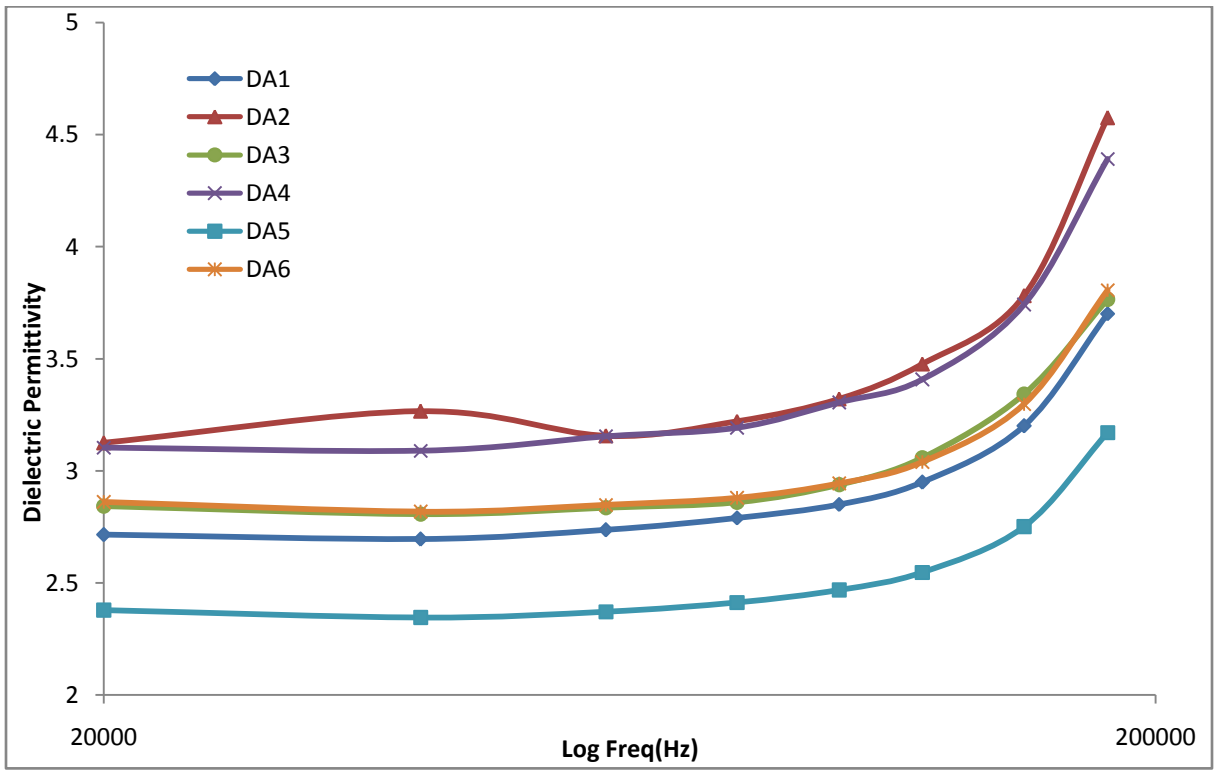

Fig 4.4.1: Dielectric permittivity of LDPE/alumina as a function of frequency for different concentration

Fig 4.4.1 Shows the frequency dependent dielectric constant LDPE/alumina at different concentrations. It is very clear from the figure that the permittivity values of the LDPE/alumina samples were fairly constant up to about 100 kHz and increases thereafter for all the samples. At frequencies between $20 - 100\ kHz$, the dielectric constant are within the range of those of non-polar polymers which PE belongs. Polar polymers at low frequencies (eg 60 Hz) generally have dielectric constants of between 3 and 9 and at high frequencies (eg 100 Hz) generally have dielectric constants of between 3 and 5. For non-polar polymer the dielectric constant is independent of the alternating current frequency because the electron polarization is effectively instantaneous hence they always have dielectric constants of less than 3 (Ahmad, 2012).

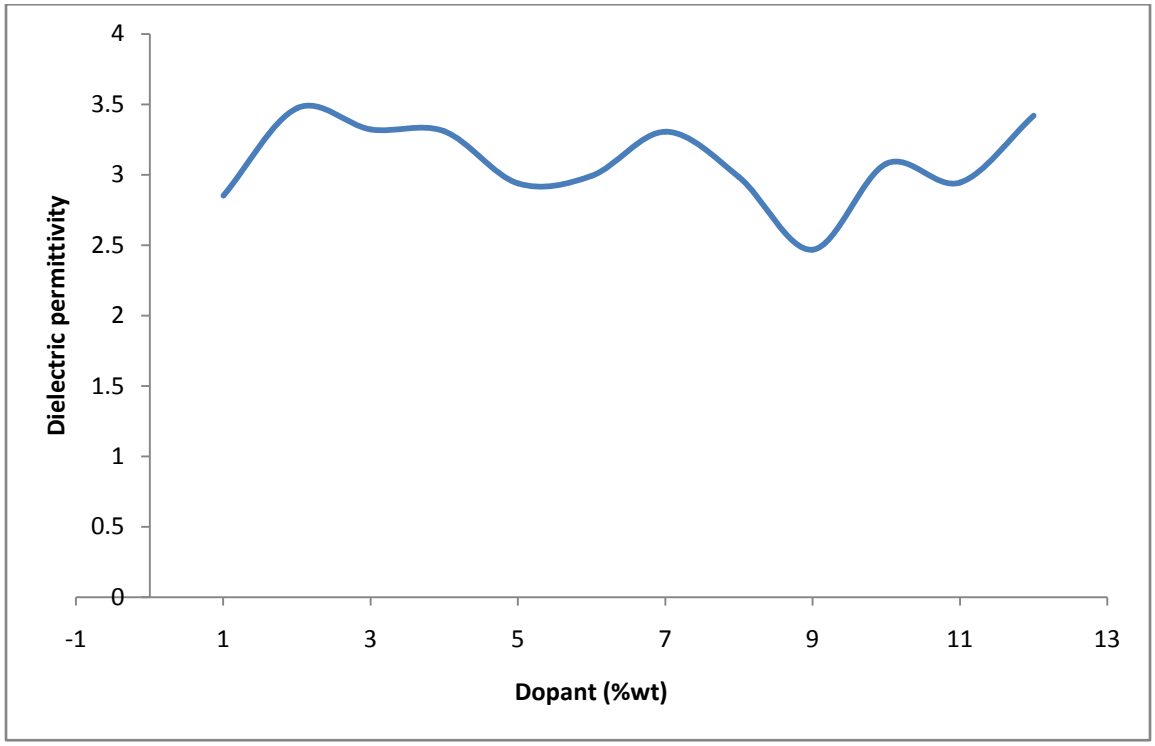

Fig 4.4.2: Variation of Permittivity with dopants in %wt at $100KHz$

Fig 4.4.2 shows the variation of permittivity with doping level at 100 kHz. The figure shows an averagely linearized progression. Except for the values at doping point 1 and 9, it is almost a linear graph.

4.2.4 Effect of frequency on conductivity

Fig 4.4.2 shows the ac conductivity of LDPE/alumina as a function of angular frequency for different concentration. The conductivity increases linearly with frequency in a logarithmic scale.

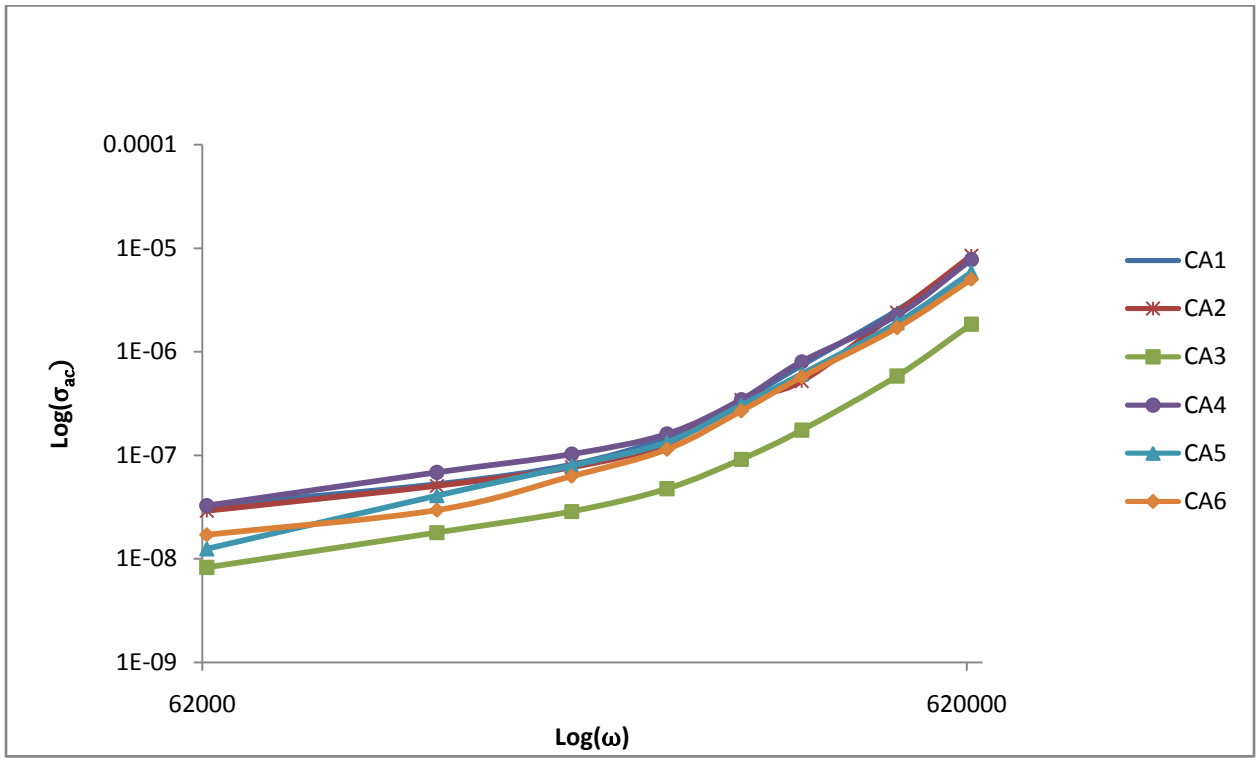

Fig 4.4.3: AC conductivity of LDPE/alumina as a function of angular frequency for different concentration

The plots generally have straight lines of two different slopes which are somewhat distinguishable at midway of the frequency region particularly at about$80KHz$.

4.2.5 Dielectric relaxation behaviour

The relaxational or deformational process of LDPE is of great importance as PE generally acts as an effective thermal insulator; thus conditions in the core of a thick sample may be very different from those in the region in contact with the walls of a mold.

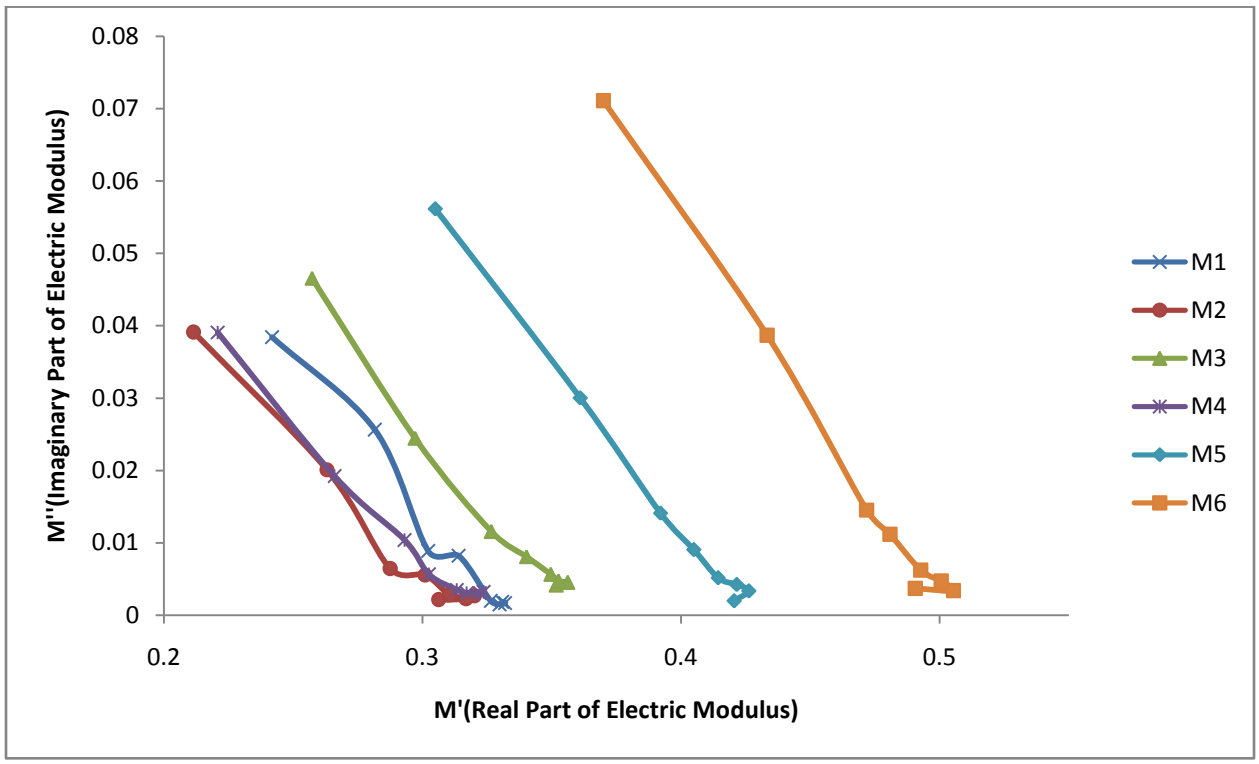

Fig4.4.4 : Argand plot between the Imaginary part (M'') versus the real part (M') of electric modulus

This becomes important because of the possibilty of experiencing creep relaxation which is very common with PE. Moreso that morphological instability can manifest itself as creep, stress relaxation and otherwise.

4.2.6 Dielectric loss with frequency

Dielectric loss result from the inability of polarization process in molecules to follow the rate of change of the oscillating applied electric field. A capacitor dissipates its stored energy through DC leakage resistance and, more importantly, the dielectric losses under an AC electric field. These account for the dissipation factor or the loss tangent, *tan δ*. This is why it is important to

examine this loss tangent as no material is free of dielectric losses, and therefore, no material is free of absorption and dispersion. All types of polarization encounter some inertia counteracting the change and, therefore, involve some dielectric loss.

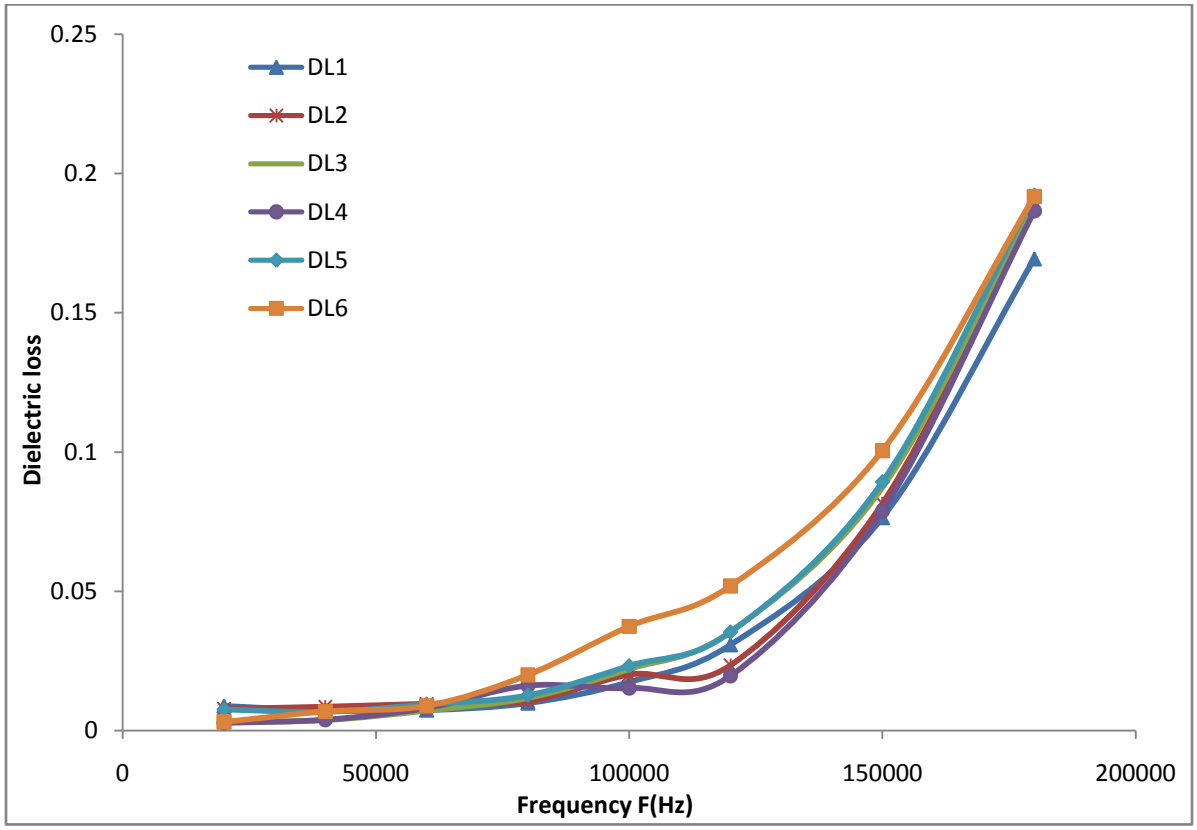

Fig 4.4.5: Plot of Dielectric loss with variation in frequency

Fig 4.4.5 shows the plot of dielectric loss with variation in frequency. The plot shows a constant loss with frequency up to 100 kHz and thereafter sharply increases.

CHAPTER FIVE

5 DISCUSSIONS

5.1 Structural Analysis

5.1.1 X-ray diffraction

The analysis of the diffractogram from fig 4.1 revealed a crystalline material though with relatively three average peaks which were quite pronounced with various intensities. These peaks which appeared at 36, 46 and 66° are the characteristic peaks of all $\gamma -$alumina. This is in conformity with the work of Seyed *et al* (2011) where their $[2\theta]$ peaks appeared at 37, 46 and 67°. The nanosized alumina was calculated to be $24.91\,nm$ using the Sherrer's equation. The comparison of the obtained XRD result with previous work confirmed the formation of γ-alumina (Seyed *et al*., 2011).

From fig 4.2, the appearance of peak at 21.9012[2θ] clearly indicates that the matrix is a semicrystalline material (Andrew, 2000). According to Mujibur *et al* (2008), the diffraction peaks at 21.5 and 23.9 of [2θ] reflection are assigned to the 110 and 200 reflections of polyethylene respectively. This makes the results obtained from this work to be in close agreement with the earlier reports. Kieran et al, (2013) worked on the characterisation of the surface and structural properties of gamma ray and electron beam irradiated LDPE reported that three crystalline peaks were identified during their experiment, these were at 21.5°, 24.3° and 36.5°. The orthorhombic phase for the peak located at 21.5° is 110, for peak 24.3° it is 200 and for peak 36.5° it is 210. These phases represent the diffraction angle which corresponds to the orthorhombic crystallite plane.

The diffractogram of LA1 and LA2 from the measurements clearly indicated a semicrystalline material with broad peaks which have no match on the ICDD data-base. This is because the existing data base does not contain a corresponding data for the new sample. As more alumina was added, i.e. LA3, LA4 and LA5, more peaks were observed emerging at [2θ] which falls within 40-60°. This shows the presence of certain impurity (alumina) which was not conspicuous at lower doping and that was also expected because the lower doping was too small to influence the matrix at that level. The doping did not shift the position of the peak any farther from the initial values. The width of the peaks did not also change with increase in doping but an increase in magnitude of the peak was observed. By doping the matrix, the LDPE is modified with the presence of nanoparticles. This implies a change in the mean atomic scattering factor on a given site (Paul, 2014). If the material is doped with a light atom, a small intensity is expected but if the atom is a heavy one like the case of alumina, there would be significant change in the magnitude of the intensity due to more scattering centres that could be created. This is because the intercalation of ions in the lattice surely leads to changes on scattering factors which will be reflected on different relative intensities. It is also possible that the change in the peak intensities is due increase in volume of nanoparticles which lead to change in the density of the crystallographic position of the samples (Paul, 2014). Generally, the [2θ] values of the peaks, for all concentrations fall virtually at the same point, except the vibrations emerging at higher [2θ] values showing the presence of alumina. This means that the alumina has interacted well with LDPE matrix and may have dispersed as isolated agglomerate rather than a network of linked particles (Maziyar and Hassan, 2014).

5.1.2 Analysis of scanning electron microscopy results (SEM)

It is of great interest that Plate 4.10 and 4.11 are gotten at different temperatures. While the former was achieved at $600℃$ the latter was obtained at $1000℃$ and both producing γ −alumina.

In plate 4.12 and 4.13, the doping mechanism was manifest showing that the material is more of intermediate than exfoliated or intercalated nanocomposites. This is due to the percentage increase in the addition of the alumina to the LDPE from 0.5wt to 1.0wt which appeared to be partially dispersed. And this is expected to be more pronounced as the addition of alumina increases gradually to 6.5%wt. In such doping mechanism, many particles of varying sizes are visible, appearing as small bright dots, fairly well dispersed across the image. This is more evident in the subsequent plates, plate 4.14 and plate 4.15 where LDPE doped with 1.5wt and 2.0wt nanoparticle. From the foregoing, further addition of the alumina in the plates (4.12 4.13, 4.14, 4.15) showed no obvious effect on the morphology by considering the amount of agglomeration on the fracture surfaces observed by SEM.

Generally, the SEM images of the samples indicate that the particles are unevenly dispersed throughout the LDPE samples. Areas with no visible particles were found in each sample. This uneven dispersion occured while using poly(methyl metecrylate)/alumina and it was explained to be due to ultimate strain and stress that results in the samples (Ash et al, 2001).

5.1.3 Fourier transform infrared spectroscopy (FTIR)

Fig 4.3 - 4.5 shows the spectra of alumina doped LDPE samples in comparison with the undoped one. LF1 is the undoped sample with about 11 to 12 prominent bands in the FTIR spectra as was obtained in an earlier report (Krimm *et al* 1956). Many of the bands obtained in this work correspond to the work of Krimm *et al* except the presence of additional weak broad bands. This is because some of the weaker bands are somewhat variable in their appearance in spectra

obtained by different observers. As the volume of alumina increased, bands corresponding to alumina began to be visible. The FTIR spectrum of alumina is between $1000 - 400\, cm^{-1}$ showing about 9 peaks. The strong peaks are located at $1029 cm^{-1}$ and others are $536 cm^{-1}$ and $472\, cm^{-1}$. And again because some of the bands are broad, FTIR peaks were identified at $1021 cm^{-1}$, $492\, cm^{-1}$ and $545\, cm^{-1}$ for different doping concentration. This result is anticipated because the alumina is within a matrix as such its peaks emergence may not appear the way it would have been if it were independently measured.

5.2 Mechanical Properties

Microhardness increases when a sample is dried or fired, rising with increased crystallinity and lamellar thickness. The increase in the samples hardness and modulus from fig 4.6 and fig 4.7 shows that these two properties have been enhanced. When the microhardness of various polymers is compared, their ranking is similar to that of the elastic modulus (Andrews, 2000).

The Modulus of elasticity for LDPE doped with alumina increased in all compositions compare to the pure LDPE whose value is $0.3\, GPa$. The result is due to the presence of more alumina filler and good interaction between the filler and the matrix. The behaviour of alumina in the LDPE as it affects modulus of elasticity according to Supri *et al* (2008), is that the nanoparticles reduces the molecular mobility of the polymer chains resulting in a less flexible material with a higher Young's modulus. This improvement in hardness and elastic modulus is encouraging because insulating materials should have certain mechanical strength to withstand vibrations depending on the area of application to which they are subjected.

5.3 Analysis of Electrical Measurement

5.3.1 Dielectric permittivity response with frequency

Generally, LDPE has dielectric constant between $(2.25 - 2.35)$ at $1\,MHz$ (Tony and David, 2005). Figure 4.4.1 shows that at lower frequency, no impact of the nanoparticle on the permittivity but as the frequency progresses, there is an increase in the loss. This is because the nanoparticle appears to have contributed to the loss at high frequency. There was an overall increase in the dielectric constant of the doped LDPE. This observed increase in the dielectric constant of LPDE after the addition of alumina is an indication that the doped material has increased ability to store electrical energy in an electric field. The concentration of the impurity does not seem to have further effect on the dielectric constant of LPDE within the concentration of the nanoparticle studied.

Addition of alumina up to about 2.5wt kept the permittivity on the increase. This may be due to interfacial interaction between the matrix and the dispersed alumina. Interfacial polarization is produced by the separation of mobile positively and negatively charged particles under an applied field, which form positive and negative space charges in the bulk of a material or at the interfaces between different materials (Kwan, 2004). These in turn modify the field distribution. The strong interfacial interactions could be due to the interfacial polarization originating from remarkable difference between the dielectric permittivity of alumina and LDPE. This interfacial polarization contributes to the increased dielectric permittivity in LDPE/alumina nanocomposites at the frequency range stated. This is found to be in good agreement with the earlier work of (Chanmal and Jog, 2009), in the case of PVDF/Clay.

This is in conformity with the work of Umasankar *et al,* (2007), where the nanocomposites have a higher dielectric constant than pure PVDF throughout the frequency range, irrespective of the clay type. The dielectric constant values increase with clay content in all the cases. It strongly

depends on the polarizability of the dielectric material; the lower the polarizability of the constituent bonds, the lower the permittivity and vice versa. Due to the nature of polyethylene, it has an extremely low interaction with electric fields and hence a very low electrical permittivity. The dissipation factors across all the samples are generally of low values ($> 0.0005\ at\ 1MHz$) as measured by (Andrew, 2000) even though the values vary from one sample to the other which are desirable, as they indicate efficient insulation. This is an indication of low power losses due to conversion of electric energy to heat, which are of great importance at high frequencies. The increase in dielectric constant in this case may be because of the charge contribution from the alumina.

From Fig 4.4.2 which shows the variation of permittivity with dopants at $100\ kHz$, it shows that the dielectric permittivity of the samples have been enhanced from the range of $(2.25 - 2.35)$ at $1MHz$ in the previous work stated, to $(2.85 - 3.47)$ at $100\ kHz$ in this present work.

5.3.2 Effect of concetration of alumina on conductivity

There is a slight increment in ac conductivity of the polymeric insulation with increase in the concentration of alumina nanoparticles. The presence of alumina must have increased the concentration of mobile ions in the samples resulting in an increase in conductivity across the doped samples. This behaviour of LDPE/alumina may be due to the semicrystalline structure of the parent matrix which allows higher mobility of the nanoparticles.

The pattern of ac conductivity within 20 kHz to 180 kHz is near linear increment. For dielectric materials, conductivity is dependent on frequency with the expression:

$$\sigma_{ac} \propto \omega^{v} \qquad 5.1$$

Where $\omega=2\pi f$ and v is the frequency exponent lying between 0 and 1. The electrical conductivity behaviour follows the universal power law represented in equation 5.1. The values of v can be determined from the linear slope of the lines. The values appeared to be increasing as frequency increases. This increase becomes pronounced at higher frequency indicating that the mobile ions involved in conductivity could easily be transferred within the polymer matrix leading to electrical conducting network formed in the LDPE/alumina sample. It is also possible that the nature of alumina, which has high electrical resistivity and relatively high thermal conductivity (Amit et al., 2012) than that of LDPE, may have contributed greatly to the increase in the conductivity of the doped LDPE with frequency.

5.3.3 Analysis of dielectric relaxation behaviour

According to Ying *et al* (2012), the relaxation behaviour of polymer chains in polyethylene is affected by the surface-area-to-volume ratio (shape) of the nanoparticle, as a result of both the interaction between nanoparticle and polymer chains. The nanoparticle induced topological changes of polymer chains surrounding the nanoparticles is also worthy of consideration. Each relaxation process requires a certain time to reach its thermodynamic equilibrium state, which is generally referred to as the relaxation time of the process. This would have been calculated using the frequency at that point if it were determined with LCR that could measure up to 1MHz.

Fig 4.4.3 shows the relaxation behaviour with slopes falling between -0.3593 to -0.5223. From the Argand plot, they all follow the same pattern of relaxation which may likely be an indication of low stress brittle failure which is usually initiated at surface or bulk inhomogeneities that act as stress concentrator and of course which the samples (LDPE/alumina) possess. This is in agreement with (Andrews, 2000) where the plot of relaxation modulus with time for medium density polyethylene at various strains at 23°C behaves in a similar manner.

5.3.4 Dielectric loss with frequency

Fig 4.4.4 shows the plot of loss tangent with variation in frequency within the range of 20 kHz to 180 kHz. At low loading (1-3%wt) it was constant, and at medium loading (3.5-6%wt), it increased sharply. The increase in the loss tangent with increase in frequency is an indication that a loss peak would have appeared if the studied frequency range is up to 1 MHz as obtained in previous work (Andrew, 2000). The analysis of the obtained results shows that dielectric loss appears to be relatively constant from 20 kHz to 80 kHz and beyond which there is a sharp increase in loss up till 180 kHz. But increase in the volumetric content of the filler alumina seems to have no pronounced effect on dielectric loss. The loss tangent appears to show no much variation in all samples across the frequency range studied. The increase in dielectric loss may have been caused polarization effect associated with increase in frequency. It is well known that dielectric loss is usually high around the relaxation or resonance frequencies of the polarisation mechanisms (Kwan, 2004). This polarisation lags behind the applied field, causing an interaction between the field and the dielectric's polarisation that result in heating up the sample as the material is subjected to higher frequency. This makes it possible for dielectric loss to dissipate energy through the movement of charges in an alternating electromagnetic field as polarisation switches direction (Kwan, 2004).

The loss also increased after remaining constant up to 80 Hz. This is may be due the fact that increase in the volumetric content of the alumina filler even though the alumina causes the growth of the number of the nanoparticles per cross sections of the composite. This behaviour was observed in the work of Huang and Jiang (2007), where PE was doped with aluminium nanocomposites showing a similar trend. It was suggested by these previous researchers that at high filler loadings, dielectric loss in polymer nanocomposite may decrease due to voids from

imperfect filler packing and solvent evaporation. This may be because a solvent is required to disperse nanofillers at a comparatively higher loading level in the polymer matrix.

CHAPTER SIX

6 SUMMARY, CONCLUSION AND RECOMMENDATIONS

6.1 Introduction

This research work focused on the synthesis and characterisation of LDPE doped with alumina. Two types of alumina were prepared, one from kaolin and the other from alum to determine which will give the highest yield and most pure. Alumina from alum gave the highest yield and of a purity of 89%. Alumina from Kaolin which gave 66% purity but in abundance was subsequently used to dope LDPE at varying concentration. This was done to be able to ascertain the degree and at what level of enhancement it caused to the dielectric permittivity in particular.

6.2 Summary of Experimental Results

Alumina has been prepared via acid leaching with kaolin and combustion sintering with alum. In the latter 89% purity was recorded with higher yield while alumina from kaolin gave 66% purity with lower yield. The two raw materials demonstrated the potential to produce alumina with different acid usage. Sherrer's equation revealed that alumina from kaolin has $24.91\,nm$ as its crystallite size while the alumina from alum gave $92.13\,nm$.

The morphology and microstructures of the samples have been examined by scanning electron microscopy. An intermediate nanocomposite material was produced. The SEM images of the samples indicate that the particles are unevenly dispersed throughout the LDPE samples; areas with no visible particles were found in each sample. XRD patterns are very consistent with all having the same [2θ] position except for the broadness of some of the peaks.

The effect of addition of alumina, with different concentrations to Low Density polyethylene (LDPE) samples has been investigated as a function of frequency at room temperature. The results revealed that both the hardness and elastic modulus have been greatly enhanced with the hardness improving from 13.5 MPa (pure LPDE) to $(14-34\ MPa)$ in this present work. As for elastic modulus, Maziyar and Hassan (2014) got a maximum of $0.48GPa$ while using carbon nanotubes (CNT). The hardness improved from $13.5MPa$ as it came in the work of Andrews (2000) to $(14-34MPa)$ in this present work. As for elastic modulus, Maziyar and Hassan (2014) got a maximum of $0.48\ GPa$ with doping LDPE/carbon nanotubes while this work produced $(0.74-1.44GPa)$.

The dielectric constant of the samples produced in this work have been enhanced from the range of $(2.25-2.35)$ at $1MHz$ in the previous work stated, to $(2.85-3.47)$ at $100\ kHz$. The filler alumina may not have any pronounced effect on the dielectric loss because at every frequency, the loss appeared to be nearly constant. Therefore increase in loss may have been caused by the variation in frequency because dielectric loss is usually high around the relaxation or resonance frequencies of the polarisation mechanisms.

6.3 General Conclusion

Going by the experimental conditions employed in this work, the followings are the major conclusions

1. γ alumina was prepared by concentrated hydrochloric acid leaching from Kaolin. This demonstrate the feasibility of producing alumina from Nigerian kaolin

2. Calcinations temperature (600℃) and calcinations time (4 hours), aside hydrochloric concentration and leaching time has a pronounced reactive effect on the alumina extraction
3. γ alumina was also prepared from alum via combustion by using potash
4. The combustion process gave a higher grade alumina than the leaching process even though the latter involves the use of various acids which makes the method more malign because of the health threat it poses.
5. The dispersion mechanism of the samples showed that an intermediate nanocomposites has been produced which may likely posses good electrical and mechanical properties.
6. FTIR showed the same pattern with peculiar peaks appearing throughout. As the concentration of dopant increases, certain peaks appeared and later disappeared showing the instability of such peaks. Some other peaks later appear as others vanish.
7. The nanoidentation result showed that the elastic modulus and hardness are largely enhanced across all the concentrations of alumina.
8. Alumina has been used to dope LDPE to principally enhance the dielectric permittivity and it was duly enhanced.
9. Dielectric permittivity at $100\ kHz$ was fairly constant across the doping points and with most values above the reference range of LDPE with non falling below the maximum value that can be gotten without doping. This is the general behaviour of all the samples at the measured frequencies.
10. Conductivity across the doping was also linearly constant and stable for all the samples.

11. There was increase in dielectric loss which may possibly decrease at a higher frequency. This initial increase after been fairly constant up to 80Hz may have been caused by the variation in frequency leading to its polarization effect.

6.4 Contributions

In this work, a shorter route using combustion method has been identified to produce alumina from alum and potash without the use of urea producing a purity of 89% and a good yield. Two sets of alumina have been produced from local contents (Kaolin and alum) with $24.91nm$ and $92.13nm$ as their crystallite sizes respectively. Alumina from alum with potash via combustion was prepared under the combustion temperature of 200℃ while alumina was gotten from kaolin through acid leaching. LDPE was successfully doped with the alumina to produce intermediate nanocomposites which possesses a good electrical and mechanical behaviour. The samples (LDPE/alumina) possessed comparatively good elastic modulus and hardness. Samples doped at 2.5, 3.0 and 3.5 wt% appeared to have most optimum behaviour in that they have the lowest dielectric loss out of all the samples produced. The samples prepared within the stated ranges also have good stability with respect to elastic modulus and hardness and may therefore be considered as a good alternative electronic substrate for polymeric applications compared to others fabricated at different percentage weights

This work has produced LDPE/alumina samples with enhanced dielectric permittivity from the range of $(2.25 - 2.35)$ at $1MHz$ to (2.45-4.91) at (20 kHz-180 kHz). The prepared samples have an average dissipation factor of 0.006228 at 20 kHz. The increase in dielectric permittivity of the samples and relatively low and stable tan delta value is an

indication of low loss which makes the material an efficient insulator compared to its matrix.

6.5 Recommendation and Future Focus

1. The use of micro screw extruder for the preparation of the samples would yield a better dispersion of the nanocomposites in the polymer matrix.
2. The difficulty to measure the frequency range above $20\,kHz$ to $1\,GHz$ with a high precision impedance analyzer that does not exist in the country as at when this work was carried out should be studied. This would give a wider spectrum and complete behaviour of the doped samples.
3. The samples should further be examined for HVDC cables insulation in order to ascertain the effects of alumina on the cable performance when carefully investigated.

7 REFERENCES

Abdul W, Al-jaleel A and Suad I. A (2006). Alumina Recovery from Iraqi Kaolinitic Clay By Hydrochloric Acid Route, *Iraqi Bulletin of Geology and Mining* Vol. 2, No 1, pp67-76

Ahmad, M.B.; Hoidy, W.H.; Ibrahim, N.A.B. & Al-Mulla, E.A.J. (2009). Modification of montmorillonite by new surfactants. *J. Eng. Appl. Sci.*, Vol.4, No. 3, 184-188.

Ahmad, Z.(Eds, Marius A. S.) (2012). *Dielectric Materials: Polymeric Dielectric Materials*, In Tech, Croatia

Ali Olad (2011). *Polymer/Clay Nanocomposites, Advances in Diverse Industrial Applications of Nanocomposites*, Dr. Boreddy Reddy (Ed.), ISBN: 978-953-307-202-9, InTech, Available from:http://www.intechopen.com/books/advances-in-diverse-industrial-applications-of nanocomposites/polymerclay- nanocomposites

Amit, S, Modi O. P., and Gaurav K. G (2012). Effect of Fuel to Oxidizer ratio on Synthesis of Alumina Powder Using Solution Combustion Technique-Aluminium Nitrate & Glycine Combination. *Advances in Applied sciences Research*, 3 (4):2151-2158

Andrew J. Peacock (2000). Handbook of Polyehtylene; Structures, properties andApplications, Marcel Dekker, inc, New York. pp. 67-113

Andrews, T. Hampton, R.N. Smedberg, A. ,(2006): "The role of degassing in XLPE power cable manufacture", IEEE Electrical Insulation Magazine, Vol. 22, No. 6, pp. 5-16

Ash, B.J., Stone, J., Rogers, D.F., Schadler, L.S., Siegel, R.W., Benicewicz, B.C., Apple, T., ,(2001). *Investigation into the Thermal and Mechanical Behavior of PMMA/Alumina Nanocomposites*, in *Filled and Nanocomposite Polymer Materials*, Book of Proceedings, Materials Research Society: Boston, MA. p. KK2.10.1-10.6.

Ashcroft, N.W. and Mermin, N.D.,(1976). *Solid State Physics*, Saunders College Publishing, 718-722.

Barbara, S. (2004). *Infrared Spectroscopy: Fundamentals and Applications*. Wiley and Sons Inc. P 18-44

Carl C. Koch (2002). Nanostructured materials: Processing, Properties and Potential Application. Noyes Publications, Norwich, NewYork, USA.

Carmen C. S., Martin W., Nathaniel T., Linda F., and Eva M., (2015). Novel Nanocomposites of Poly(lauryl methacrylate)-Grafted Al_2O_3 Nanoparticles in LDPE**,** *ACS Appl. Mater. Interfaces*, 7 (46), pp 25669–25678

Chanmal C.V and Jog J.P. (2009). A Study of Dielectric Behaviour of PVDF/clay Nanocomposites. e-Polymers, no. 112, http://www.e-polymers.org

ISSN 1618-7229

Cheng, K. C.; Lin, C. M.; Wang, S. F.; Lin, S. T.; Yang, C. F.,(2007). Dielectric properties of epoxy resin-barium titanate composites at high frequency. *Materials Letters***,** 61, (3), 757-760.

Chen G., Sadipe J.T., Zhuang Y., Zhang C. and Stevens G. C. (2009). Conduction in Linear-low Density Polyethylene Nanodielectric Materials, proceedings of the 9th International Conference of properties and Applications of Dielectric Materials, Howbin China 845-848

Ching Y. C., Song N. L,. Luqman C. A., Thomas S. Y. C.,Azowa I., and Chantara T. R. (2012). "Characterization of Mechanical Properties: Low-Density Polyethylene Nanocomposite Using Nanoalumina Particle as Filler, *Journal of Nanomaterials* Hindawi Publishing Corporation, Article ID 215978.

Chigwada, G.; Wang, D.; Jiang, D.D. & Wilkie C.A. (2006). Styrenic nanocomposites prepared using a novel biphenyl-containing modified clay. *Polym. Degrad. Stab.*, Vol. 91, 755-762.

Christopher C., Keith N. J., Linda S. S. Daniel S. (2010). Polyamideimide-alumina Nanocomposites for high temperatures, *International Conference on Solid Dielectrics, Potsdam, Germany.*

Cicek Karsal (2008). Preparation and Physical Characterization of Clay/EPDM Nanocomposites Unpublished Thesis Submitted to the Graduate School of Engineering and Sciences of İzmir Institute of Technology in Partial Fulfillment of the Requirements for the Degree of Master of Science in Material Science and Engineering

Ciprari D. L., (2004). Mechanical Characterization of Polymer Nanocomposites and the Role of Interphase, An MSc Thesis: Georgia Institute of Technology pp 8-32

Cole K. S., and Cole R. H., (1941). 'Dispersion and adsorption in dielectrics', *J. Chem. Rev.* **9 (**341–352),

Cullity B. D. and Stock S.R., (2001). Element of X-Ray Diffraction, 3rd Ed Prentice-Hall Inc, P 167-1717

Dang, Z. M.; Shen, Y.; Nan, C. W.,(2002). Dielectric behavior of three-phase percolative Ni- BaTiO3/polyvinylidene fluoride composites. *Applied Physics Letters***,** 81, (25), 4814-4816.

Daniel M. Dabbs, Nan Yao and Ilhan A. Aksay(1999). *Journal of Nanoparticle Research* 1**:** 127–130,

Davidson D. W., and Cole R. H., (1951).'Dielectric relaxation in Glycerol, Propylene Glycol, and n-Propanol', *J. Chem. Phys.* **19**, 1484–1490

Dissado L. A. and Fothergill J. C.,(1992). *Electrical Degradation and Breakdown in Polymers*, Peter Peregrinus, London pp 19-50

Durmus A., Kasgoz A,. and Macosko C. W.,(2008) "Mechanical properties of linear low-density polyethylene (LLDPE)/claynanocomposites: estimation of aspect ratio and interfacial strength by composite models," *Journal of MacromolecularScience B*, vol. 47, no. 3, pp. 608–619, 2008

Ellis, T.; D'Angelo, J. 2003. Thermal and Mechanical Properties of a Polypropylene. Nanocomposite. *Journal of Applied Polymer Science*, 90: 1639–1647

Fahrner W. R (2005). Nanotechnology and Nanoelectronics, Library of Congress Control Number: 2004109048 ISBN 3-540-22452-1 Springer Berlin Heidelberg New York. Pp 107-118

Forthergill J, C, Leonard A, D, and Keith N, (2003). Nanocomposite Materials for Dielectric Strucures. Fianl Report for EPSRC Grant GR/R71788/01

Giannelis, E.P., Mehtora, V., Vassiliou, J.K., Shull, R.D., MacMichael, R.D., and Ziolo, R.F.(1994), *Nanophase Materials* (Eds. Hadjipanayis, G.C. and Siegel, R.W.) Kluwer Academic Publishers, the Netherlands 197-204.

Giannelis, E.P. (1996). Polymer layered silicate nanocomposites. *Advanced. Materials.*, Vol. 8, 29–35.

Giulio M., Paola P., Silvia R., Alessandro D. and Laura M. (2010). Effect of various alumina nano-fillers on the thermal and mechanical behaviour of low-density polyethylene–Al_2O_3 composites *Polymer International* Volume 59, Issue 8, pages 1084–1089

Goldstein, J.I., Newbury, D. E., Echlin, P., Joy, D.C.,(1992) *Scanning Electron Microscopy and X-Ray Microanalysis*, New York: Plenum Press

Greene, M.; Kinser, C.; Kramer, D.; Pingree, L.; Hersam, M. 2004. Application of Scanning Probe Microscopy to the Characterization and Fabrication of Hybrid Nanomaterials. *Microscopy Research and Technique* 64:415–434

Greg A. (1997). *LCR / Impedance Measurement Basic*, Hewlett-Packard Company © pp 5-11

Hahn, J.(2nd ed.)(1988).International Tables of crystallography, Brief Teaching Edition of Vol. A , Kluwer Academic Press, New York pp 8

Hari S. N., (Eds) (2002). Nanostructured Materials and Nanotechnology, Academic Press Harcourt Place, 32 Jamestown Road, London NWl 7BY, UK http://www.academicpress.com p321

Harvriliak S and Negami S.,(1966). "A complex plane analysis of dispersion in some polymer systems", *Journal of Polymer Science* C 14, 99,

Havriliak, S. and Negami, S.,(1967). "A complex plane representation of dielectric and mechanical relaxation processes in some polymers", Polymer, 8 (4), pp. 161

Huang X. Y., and Jiang P. K., (2007). Electrical properties of polyethylene/aluminum nanocomposites, *Journal of Applied Physics 102, 124103*

Inouye H. and Kirschner D. A. (1997). X-Ray Diffraction Analysis of Scrapie Priori intermediate and folded Structure in a Peptide containing two putative Alpha-Helics, *Journal of Molecular Biology*, 268, 375-389

James P. Runt and John J. Fitzgerald, (1999). *Dielectric Spectroscopy of Polymeric Materials: Fundamentals and Applications*, Book of Proceedings, American Chemical Society

Jenney Ngu L. S. (2010). Characterization of Mechanical, Morphological and Thermal properties of Low Density Polyethylene Nanocomposites using Alumina Nanoparticles as Filler, Unpublished Thesis submitted to the School of Graduate Studies, Universiti Putra Malaysia, in fulfilment of the requirement for the Degree of Master of Science

Jordan, J.; Jacob, K. I.; Tannenbaum, R.; Sharaf, M. A. & Jasiuk, I. (2005). Experimental trends in polymer nanocomposites-a review. Journal *Material Science and Engineering. A*, Vol. 393, 1-11.

Jeffrey J, Karl I. J, Rina T, Mohammed A. S, Iwona J(2005). *Experimental Trends in Polymer Nanocomposites-A Review*, Journal: Materials Science and Engineering A-structural Materials Properties Microstructure and Processing - Material Science Engineering A-structure materials , vol. 393, no. 1, pp. 1-11,

Khumalo V. M., Karger-Kocsis J., and Thomann R. (2010). Polyethylene/synthetic boehmite alumina nanocomposites: Structure, thermal and rheological properties, *eXPRESS Polymer Letters* Vol.4, No.5, 264–274

Ki Hyun L, In Kyu S and Byoung C. K.(2008). *The rheological properties of poly(vinylidene fluoride-co-hexafluoropropylene) solutions in dimethyl acetamide*. Korea-Australia Rheology Journal. Vol. 20, No. 4, pp. 213-220

Kieran A. M, James E. K, Brian M, Olivier V., Damien R., Richard C., Clement L. H. (2013): Characterisation of the Surface and Structural Properties of Gamma Ray and Electron Beam Irradiated Low Density Polyethylene, *International Journal of Material Science (IJMSCI) Volume 3 Issue 1*

Kota, R.; Ali, A. F.; Lee, B. I.; Sychov, M. M.,(2007). Dielectric constant of barium titanate/cyanoethyl ester of polyvinyl alcohol composite in comparison with the existing theoretical models. *Microelectronic Engineering***,** 84, (12), 2853-2858

Kreuger F. H, (1965). *Discharge Detection in High Voltage Equipment*, (American Elsevier, New York) pp5-8

Krimm, S., Liang C. Y., and Sutherland, G. B. B. M. (1956). Infrared Spectra of

High Polymers. II. Polyethylene, *The Journal of Chemical Physics Volume 25. Number 3*

Kulek, J.; Szafraniak, I.; Hilczer, B.; Polomska, M.,(2007). Dielectric and pyroelectric response of PVDF loaded with BaTiO3 obtained by mechanosynthesis. *Journal of Non-Crystalline Solids* **,** 353, (47-51), 4448-4452.

Kumar A.P.; Depan, D.; Tomer N.S. & Singh, R.P. (2009). Nanoscale particles for polymer degradation and stabilization-Trends and future perspectives. *Prog. Polym. Sci.*, Vol. 34, 479-515.

Kwan Chi Kao,(2004). D*ielectric Phenomena in Solids*, Elsevier Academic Press UK

LeBaron, P.C.; Wang, Z. & Pinnavaia, T.J. (1999). Polymer-layered silicate nanocomposites: an overview. *Appl. Clay Sci.*, Vol. 15, 11-29

Li Y. C,, Tjong S. C, Li R. K. Y (2011). *Dielectric properties of binary polyvinylidene fluoride/barium titanate nanocomposites and their nanographite doped hybrids* eXPRESS Polymer Letters Vol.5, No.6 (2011) 526–534

Liqiang C. and Seong I. W (2008). Preparation and Characterization of Polyehtylene (PE)/Clay nanocomposites by in situ Polymerization with Vanadium-based Intercalation catalyst, *Polymer Bulletin* 61, 453-460

Maziyar S, Hassan S.(2014). Mechanical and electrical properties of low density polyethylene filled with carbon nanotubes, 2nd International Conference on Structural Nano Composites , IOP Conf. Series: Materials Science and Engineering 64, 012001

Mehdi H. A., Gity M. M. S, Hossein N. & Amir B. (2015). Polylactide/Polyethylene/Organoclay Blend Nanocomposites: Structure, Mechanical and Thermal Properties, *Polymer-Plastics Technology and Engineering* 53:13, 1417-1424

Oliver C. Wells (1974) Scanning Electron Microscopy;; McGraw Hill © pp20-24

Panda, R. K.; Szary, P. J.; Maher, A.; Safari, A.(1998). *Piezoelectric ceramic-polymer*

composites for weigh-in-motion sensors, Smart Structures and Materials**,** SanDiego, CA, USA, p 127-134.

Paul F. F.(2014). A new theory for X-ray diffraction, *Foundations and Advances*, Acta Crystallographica Section A, ISSN 2053-2733

Paul, D.R. and Robeson L.M. (2008). Polymer nanotechnology: Nanocomposites. *Polymer*, Vol. 49, 3187-3204.

Pavlidou, S. and Papaspyrides, C.D. (2008). A review on polymer-layered silicate nanocompopsites. *Prog. Polym. Sci.*, Vol. 32, 1119-1198.

Pedrazzoli D., Ceccato R., Karger-Kocsis J and Pegoretti A (2013). Viscoelastic Behaviour and Fracture Toughness of Linear-low-Density Polyethylene Reinforced with Synthetic Boehmite Alumina Nanoparticles, *eXPRESS Polymer Letters Vol.7, No.8, 652–666.*

Priya L and Jog J.(2002). *Journal of Polymer Science Part B Polymer Phys* ;40:1682–9
.

Priya L and Jog J.(2003). *Journal of Polymer Science Part B Polymer Phys* ;41:31–8.

Quang T. N and Donald G. B (2006). *Preparation of Polymer–Clay Nanocomposites and Their Properties.* Advances in Polymer Technology, Vol. 25, No. 4, 270–285

Ramajo, L.; Reboredo, M. and Castro, M.,(2005). Dielectric response and relaxation phenomena in composites of epoxy resin with BaTiO3 particles. *Composites Part A***,** 36, (9), 1267-1274.

Rao C. N. R. , A. Muller and A. K. Cheetham (Eds). (2004). The Chemistry of Nanomaterials. Synthesis, Properties and Applications., Copyright @ 2004 WILEY-VCH Verlag GmbH & Co. KGaA, Weinheim ISBN: 3-527-30686-2

Raw Material Research and Development Council (1997). *Occurence, Development and Prove Reserve of Some Non-Metallic Minerals in Nigeria*, Lagos Mufademic Press pg 256

Robert, M. S., Francis, S. W., and David, J. K., (2005). Spectrometric Identification of Organic Compounds. John Wiley and Sons, Inc U S A pp72-75

Schroeder P., (2003). "Kaolin" New Georgia Encyclopedia. Retrieved 01-08-2008 https://en.m.wikipedia.org/wiki/kaolinite.

Seyed A. H., Aligholi N. & Dariush S (2011). Production of γ-Alumina from Kaolin, *Open Journal of Physical Chemistry*, 1, 23-27

Siegel, R.W. and Fougere, G.E.(1995), *Material Research Society. Symposium Proc*eedings **362**, 219-229.

Siegel, R.W. and Fougere, G.E.,(1994) *Nanophase Materials* (Eds. Hadjipanayis, G.C. and Siegel, R.W.) Kluwer Academic Publishers, the Netherlands, 233-261.

Song Y, Zhao Z, Yu W, Li B & Chen X (2007). Morphological structures of poly(vinylidene fluoride)/montmorillonite nanocomposites, *Science in China Series B: Chemistry* vol. 50 no. 6, 790-796

Supri A.G, H. Salmah, and K. Hazwan (2008). Low Density Polyethylene-Nanoclay Composites: The Effect of Poly(acrylic acid) on Mechanical Properties, XRD, Morphology Properties andWater Absorption. *Malaysian Polymer Journal (MPJ) Vol 3 No. 2, p 39-53*

Thostenson, E.T.; Li, C. & Chou, T.W. (2005). Nanocomposites in context. *Compos. Sci. Technol.*, Vol. 65, 491-516.

Tong Liu, (2010). Dielectric Spectroscopy of Very Low Loss Model Power Cables, Thesis submitted for the degree of Doctor of Philosophy at the University of Leicester

Tony Blythe and David Bloor (2005). *Electrical Properties of Polymers*, Cambridge University Press.

Umasankar P. T, Milind V. M, Khakhar D. V., Ashok M (2007). Studies on poly(vinylidene fluoride)–clay nanocomposites:Effect of different clay modifiers- A Paper from the Department of Chemical Engineering, Indian Institute of Technology Bombay, India

Usuki, A.; Kawasumi, M.; Kojima, Y.; Okada, A.; Kurauchi, T. & Kamigaito, O. J. (1993). Swelling behavior of montmorillonite cation exchanged for V-amino acids by Ecaprolactam.*Journal* of *Mateial Research.*, Vol. 8, No.5, 1174

Valavala .K. and Odegard G.M. (2005). Modeling Techniques For Determination of Mechanical Properties of Polymer Nanocomposites.

Wohlfarth, E.P.,(1980). *Ferromagnetic Materials vol 2*., North-Holland Publishing Company, Amsterdam, 436-444.

William G. E. Aldo B. A. Jinwen Z (2005). Polymer Nanocomposites: Synthetic And Natural Fillers a Review, Maderas. Ciencia y tecnología 7(3): 159-178,

Ying L, Martin K, and Wing Kam L (2012). Nanoparticle Geometrical Effect on Structure, Dynamics and Anisotropic Viscosity of Polyethylene Nanocomposites, *Macromolecules*, 45, 2099−2112, American Chemical Society (ACS) Publications.

Zhi-Qiang F, Qi-Chang H, Qingfeng Z and Pierre Joli (2010). Handbook of Nanophysics, K. Sattler (eds.), Taylor & Francis, pp 1-26